

CZECH TECHNICAL UNIVERSITY IN PRAGUE
FACULTY OF MECHANICAL ENGINEERING
DEPARTMENT OF ENVIRONMENTAL ENGINEERING

DUAL-FUNCTION SOLAR COLLECTOR

DIPLOMA THESIS

ABHINAV MOHITE

2 – EE – 2016

Czech Technical University in Prague
Faculty of Mechanical Engineering

Department of Environmental Engineering Academic year: 2015/2016

MASTER THESIS ASSIGNMENT

Student name: Bc. Abhinav MOHITE

Study program: Mechanical Engineering

Study field: Environmental Engineering

Thesis title: Dual-Function Solar Collector

Elaboration guidelines:

Design a solar thermal collector to be used in two modes – as water heater and air heater. The design will be based on finned tube heat exchanger. The collector will be intended mostly for roof installations. Air flow through the collector should be 80 to 160 m³/h per m² of nominal collector area. Optimize the spacing of fins with respect to the air passage pressure loss and the collector heat loss by radiation. Design a suitable air inlet for the collector so that the air flow is well distributed over the collector width.

Extent of graphic work: Graphic presentation of results.

Extent of textual report: Detailed technical report including the description of applied methods and the discussion of results.

Literature:

- 1) Incropera F.P., Dewitt D.P. et al. *Fundamentals of heat and mass transfer*. 6th ed. Hoboken : Wiley, 2007.
- 2) Siegel R., Howell J.R. *Thermal radiation heat transfer*. 4th ed. New York : Taylor and Francis, 2002.
- 3) He W., Xiaoqiang H. et al. CFD and comparative study on the dual-function solar collectors with and without tile-shaped covers in water heating mode. *Renewable Energy* 86 (2016), p. 1205-1214.

Thesis supervisor: Ing. Martin Barták, Ph.D.

Consultant: Doc. Ing. Tomáš Matuška, Ph.D.

Assignment issue date: 18th April 2016

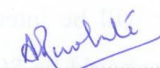
Thesis due date: 29th June 2016


If the student does not submit his/her thesis by the due date and provides a reasonable excuse in writing, and the excuse is accepted by the dean, the dean appoints a substitute deadline for the thesis submission. If the student does not deliver a proper letter of excuse or if the excuse is not accepted by the dean, the student is eligible for a second thesis enrolment.

The student is aware that the thesis has to be accomplished through an independent and unassisted student's work, supported only by recognized consultations. Literature and other information resources as well as consultants' names have to be acknowledged in the thesis.

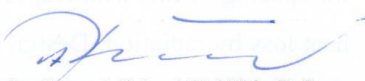
Thesis assignment received:

25 - April - 2016
Date


Student


Doc. Ing. Vladimír Zmrhal, Ph.D.
Head of the Department




Prof. Ing. Michael Valášek, DrSc.
Dean of the Faculty

Prague, 18th April 2016

I declare that this diploma thesis entitled "**Dual-Function Solar Collector**" is my own work performed under the supervision of Ing.Martin Bartak, Ph.D with the use of the literature presented at the end of my diploma thesis in the list of references.

In Prague 29.06.2016

Abhinav Mohite

Abstract

The thesis deals with a dual-function solar collector, which would perform the function of heating the air during the winter and heating up the water during the summer. In order to achieve a reasonably priced collector, the design approach is motivated by the utilization of components that are commercially available. The collector is based on fin-tube water-air heat exchanger, which is normally produced for air handling units. Several design options were analysed using manual calculations and CFD simulations. A number of models were created and simulated in ANSYS Fluent software to study the performance of both the water and air side of the collector. The analysis included fluid flow with heat transfer by conduction, convection and radiation, including solar load calculations. Satisfactory results were obtained for the air side, the model for the water side did not work properly. Conclusions were made regarding the influence of fin spacing on pressure losses and radiative heat losses and regarding the surface selectivity with respect to solar radiation.

Table of contents

1. INTRODUCTION	11
2. BACKGROUND AND LITERATURE REVIEW	13
2.1 Photovoltaic/thermal hybrid solar collectors.....	13
2.2 Air and water thermal collector	15
2.3 Triple function photovoltaic/thermal solar collector	21
3. CONCEPT FOR THE CURRENT DESIGN	24
3.1 Air inlet design	26
4. PRINCIPLES OF CFD	27
4.1 Flow Calculation	28
4.2 Radiation model	29
4.3 Solar Load Model.....	30
4.4 Solar Calculator	31
5. MANUAL CALCULATIONS	32
5.1 Heat loss by Radiation	32
5.2 Pressure loss across the collector	38
6. CFD MODEL	41
6.1 Modelling.....	41
6.1.1 Air side geometry	41
6.1.2 Water Side Geometry	43
6.2 Meshing.....	45
6.2.1 Meshing for air side model.....	45
6.2.2 Meshing for water model.....	47
6.3 Boundary Conditions.....	49
6.3.1 Air side model boundary conditions.....	49
6.3.2 Water side model.....	50
7. RESULTS	52
7.1 Air side model (4.32 mm) for summer conditions	52
7.2 Air side model (4.32 mm) for winter	53
7.3 Air side model (1.41 mm) for winter	54
7.4 Water side model.....	56
7.5 Radiation gains and losses for winter conditions	56
7.6 Pressure loss across the air side.....	58

7.7 Radiation losses through the fins.....	59
8. CONCLUSION.....	60
9. BIBLIOGRAPHY.....	62

List of Figures

Figure 1 : Basic construction of PV/T collectors (Chow, 2009)	14
Figure 2 : Different construction of air PV/T collectors (Chow, 2009).....	14
Figure 3 : Different construction of water PV/T collectors. (Chow, 2009)	15
Figure 4 : General design of DPSC (Assari, 2009)	16
Figure 5: Schematic of the proposed Dual Purpose Solar Collector (Venu, 2013)	17
Figure 6 : Illustrative diagrams of the building-integrated dual-function solar collector system showing: (a) the water heating circuit and (b) the passive space heating (sectional view).	18
Figure 7 : Schematic of DPSC (Assari, 2009)	19
Figure 8 : Three kinds of air channels, (a) no fin, (b) with straight fin, (c) with triangular fin. (Assari, 2009)	19
Figure 9 : Fig. 1.9 The structure of the modified dual-function collector (Jinwei, 2011)	20
Figure 10 : Schematic of the tri-functional PV/T collector.....	22
Figure 11 : Basic structure of collector	24
Figure 12 : Overall dimensions.....	24
Figure 13 : Production capabilities by Lloyd coils (www.lloydcoils.eu)	25
Figure 14 : Air inlet (slot diffuser) construction.....	26
Figure 15 : Slot diffuser dimensions.....	26
Figure 16 : The structure of the modified dual-function collector with absorber plate at bottom and rectangular fins. (www.electronics-cooling.com).....	32
Figure 17 : The 2-D structure of a single channel	33
Figure 18 : Surfaces 1 and 2 with a common edge	34
Figure 19 : F_{14} vs h/w	35
Figure 20 : The surfaces 2 and 3.	35
Figure 21 : Graph for F_{23} vs h/w	36
Figure 22 : Heat radiation circuit.	37
Figure 23 : Rectangular Fin structure.....	39
Figure 24: Collector with wide gap (4.32 mm).....	41
Figure 25 : Collector with narrow gap (1.41 mm).....	42
Figure 26 : Front View of the fins and the pipe (both collector)	42
Figure 27 : Detail View of the inlet, top glass cover and base absorber plate.	42
Figure 28 : Collector with wide gap	43
Figure 29 : Inlet, Glass top and Fins of collector.	44
Figure 30 : Meshing details of air side model.	46
Figure 31 : Mesh model	46
Figure 32 : Mesh Model for water side model	48
Figure 33 : Mesh Model in fluent.....	48
Figure 34 : Rise in air temperatures vs time (21 st June).....	52
Figure 35 : Temperature rise vs hours (21 st December) for wide gap	53
Figure 36 : Temperature rise vs hours (21 st December) for narrow gap	54
Figure 37 : Overall velocity (m/s) profile for air.....	55
Figure 38 : Velocity (m/s) profile near the outlet of the collector.....	55
Figure 39 : Temperature (K) profile over the fins	55

Figure 40 : Gains and losses for collectors with selective coating on 21 st December	57
Figure 41 : Gains and losses for collectors with non-selective coating 21 st December.....	58
Figure 42 : Pressure drop along fins vs space between fins	58
Figure 43 : Radiation heat loss from single air channel.	59
Figure 44 : Radiation loss vs fin spacing.....	59

List of Symbols

σ	Stefan-Boltzmann constant ($5.670367 \times 10^{-8} \text{ Wm}^{-2}\text{K}^{-4}$)
T	Temperature (K)
J	Radiosity (W/m^2)
ε	Emissivity (-)
F_{i-j}	View factor (-)
h	Height of the fin (m)
w	Width of the fin (m)
Re	Reynolds Number (-)
D_h	Hydraulic diameter (m)
P	Pressure (Pa)
ρ	Density (kg/m^3)
μ	Dynamic viscosity (Ns/m^2)
Ψ	Coefficient of reflectivity (-)
α	Coefficient of absorptivity (-)
τ	Coefficient of transmissivity (-)

1. INTRODUCTION

A growing demand for energy, the security of supply of fossil fuels and the international agreements to mitigate climate change are key issues of the modern society. These developments have drastically increased the necessity of large scale implementation of renewable energy technologies over the past two decennia and will continue to do so in the near future.

Energy consumed in buildings accounts for approximately 30–40 % of the global energy consumption. Some major consumptions are lighting, ventilating, space heating/cooling, and water heating. Heat generation and electricity generation have a negative impact on the environment and represent a major human contribution to global climate change.

Over the past four decades, solar thermal systems have gained wide spread applications in building sector globally. By the end of 2010, the solar thermal collector capacity in operation worldwide equalled 195.8 GWth ('th' stands for 'thermal'). According to the data issued by International Energy Agency, by 2020, the EU will be expected to reach a total operational solar thermal capacity of around 102 GW.

To fight against the worldwide deteriorating energy wastage and pollution problems, much effort in the building sector has been on promoting solar energy utilization. To this, the applications of solar thermal technology – with passive space heating and water heating as the two major approaches – have been highly successful.

Among the solar thermal technology, the flat-plate solar collectors have been widely used as air heaters or water heaters. In modern day houses, high quality insulation is used thus the major energy losses are ventilation losses. The solar air heaters have been used to compensate for the losses by ventilation. In order to increase the annual application of solar energy, a dual-function solar collector is being designed and simulated in this thesis. This collector can generate not only hot water for domestic purposes during summer but also be used for compensating the ventilation losses in winter. Such integrated design makes it more cost-effective than those conventional systems solely for solar air heating.

The thesis deals with the design of a dual-function (water and air) solar thermal collector. Some aspects of the fluid flow and heat transfer in different parts of the collector are investigated using manual calculations and CFD simulations. ANSYS Fluent is used as the simulation software.

The collector design is based on the idea to utilize components which are being commercially produced in order to make the new product as cheap as possible. After studying the design of solar collectors and heat exchangers available on the market, a design similar to the fin-tube heat exchanger was selected. A number of model variants were prepared and simulated in ANSYS Fluent. The simulations incorporated heat transfer by conduction, convection and radiation, including solar load calculations for selected summer and winter days at a location in Prague, Czech Republic.

2. BACKGROUND AND LITERATURE REVIEW

A hybrid solar collector is a device that utilizes incident solar radiation to obtain clean energy in more than one way for a wide usage. In a hybrid solar collector, energy is converted into thermal energy using two different fluids or solar thermal collector and photovoltaics working together in different combinations on converting solar radiation into thermal and electrical energy. Such integrated design makes it more cost-effective than those conventional systems solely for solar water heating or passive space heating or electricity generation.

These designs can be classified into

- Photovoltaic/Thermal collectors.
- Air and water thermal collector.
- Triple function photovoltaic/thermal solar collector.

2.1 Photovoltaic/thermal hybrid solar collectors

A photovoltaic/thermal hybrid solar system (or PVT system for simplicity) is a combination of photovoltaic (PV) and solar thermal components/systems which produce both electricity and heat from one integrated component or system. In other words, PV is used as (part of) the thermal absorber. There are alternative approaches in PVT integration. Among many others, there can be selections among air, water or evaporative collectors, monocrystalline/polycrystalline/amorphous silicon (c-Si/pc-Si/ a-Si) or thin-film solar cells, flat-plate or concentrator types, glazed or unglazed panels, natural or forced fluid flow, standalone or building-integrated features, etc. Accordingly, available installations are ranging from PVT air and/or water pre-heating system to hot water supply through PV

integrated heat pump, and to actively-cooled PV concentrator through the use of economical reflectors. (Chow, 2009)

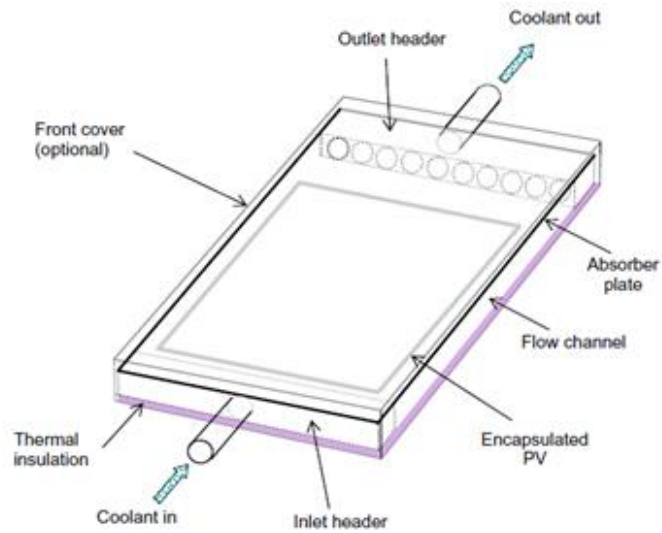


Figure 1 : Basic construction of PV/T collectors (Chow, 2009)

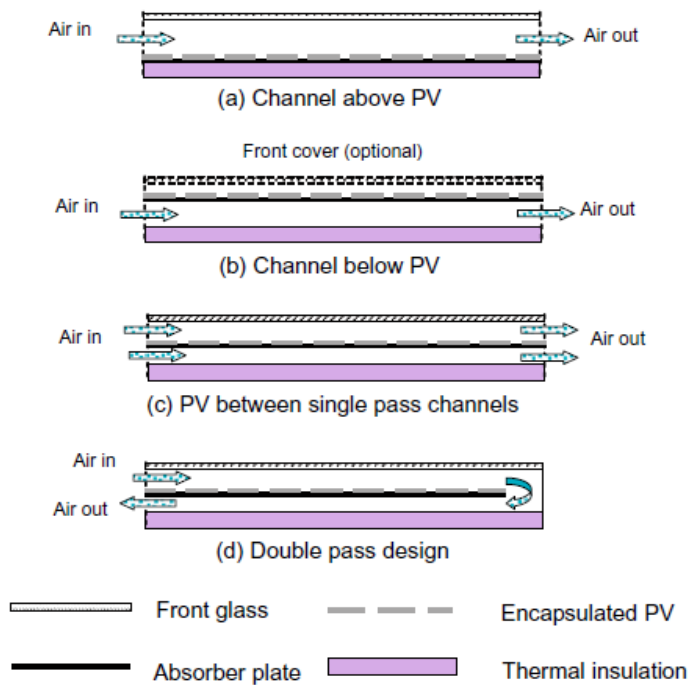


Figure 2 : Different construction of air PV/T collectors (Chow, 2009)

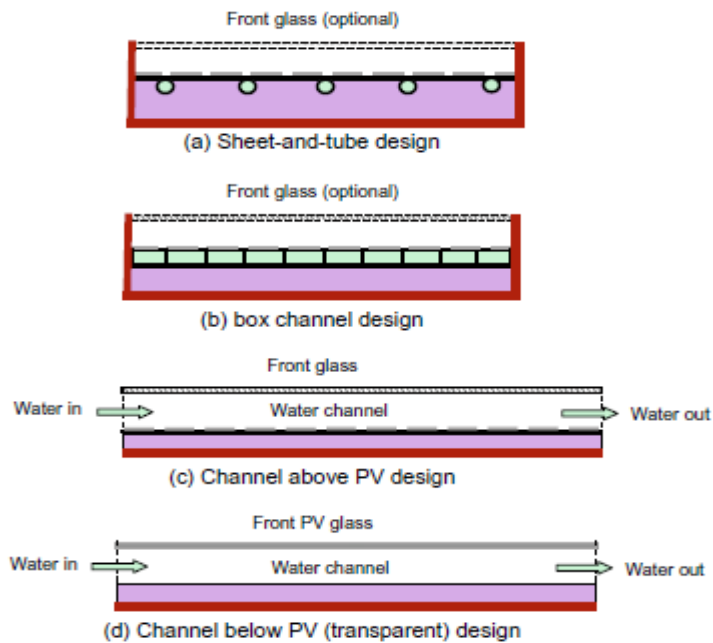


Figure 3 : Different construction of water PV/T collectors. (Chow, 2009)

2.2 Air and water thermal collector

It is modified from the conventional flat-plate collector by broadening the air gap between the absorber plate and the glass cover on top. The absorber is usually a sheet of high-thermal conductivity metal with tubes or ducts either integrated or attached. The absorber plates can be unfilled or wavy or finned to create air turbulence that helps the heat to pass from the plate to the air. Two vents are added to it, one for the inlet of cold air and the other for the outlet of the heated air. All this is packed in an insulated box which provides structure and sealing and reduces heat loss from the back or sides of the collector.

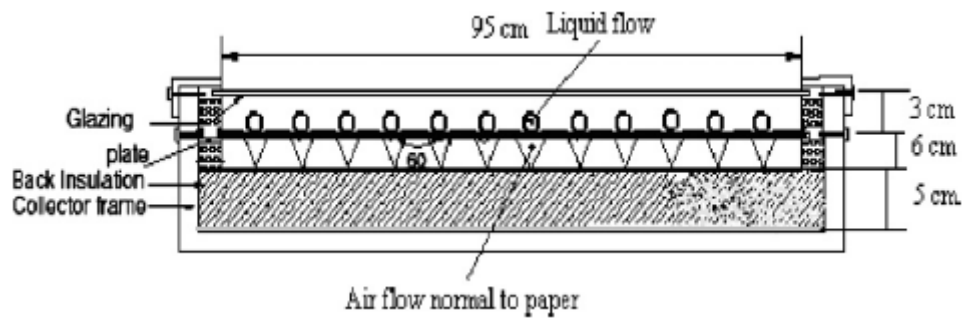


Figure 4 : General design of DPSC (Assari, 2009)

This system not only performs passive space heating in cold winter or crop drying in harvest season, but also as a water heating collector(Wei,2016). The problem of water-freezing in winter can be solved and also solar air heaters are relatively limited in their thermal performance due to the low density, volumetric heat capacity and heat conductivity of air. There has been many research work done on air collectors or only on water solar thermal collectors. But there is very less work seen on dual purpose solar collector (DPSC). However, conventional solar air collectors have the inherent disadvantage of low thermal efficiency. Such integrated design makes it more cost-effective than those conventional systems solely for solar water heating or passive space heating. The efficiency achieved by using the dual purpose (DPS) solar heating system is about 3 to 5 % higher compared to that of a single purpose solar water system (Qahtan, 2015).

In experimental study of the performance of the dual purpose solar collector (Saleh, 2014). A flat plate dual solar collector with dimensions (120×80×15) cm was used for heating the test space with dimensions (2×2×2.5) m. It was concluded from their work, that the DPSC could be used as a heat exchanger for space heating at night. Air and water temperature difference of dual solar collector increased when solar radiation increased. The effectiveness of water circuit is greater than air circuit effectiveness in air-water heat exchanger. Using dual flat plate solar collector as heat exchanger will reduce cost and time.

For increasing the efficiency of the DPSC, simulation studies on porous medium integrated dual purpose solar collector was performed (Venu, 2013). A CFD simulation study was undertaken to investigate the integration of a porous matrix to dual purpose collectors. The porous matrix is incorporated below the absorber plate of the collector to improve the thermal performance of the overall system. The total thermal efficiency of the modified collector is found to vary from 34.60 % to 46.03 % over inlet water temperature range of 30°C to 90°C.

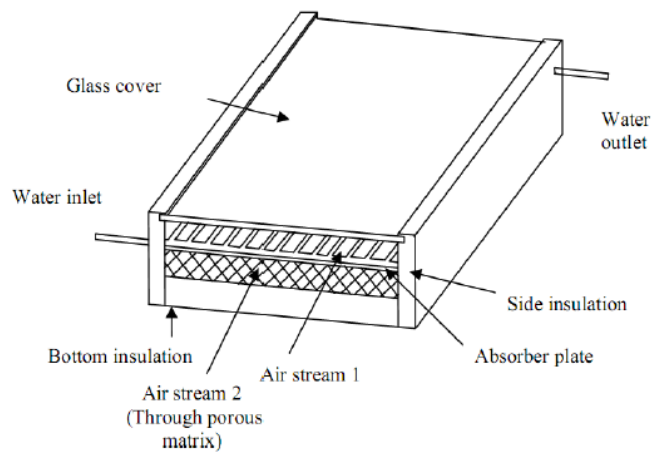


Figure 5: Schematic of the proposed Dual Purpose Solar Collector (Venu, 2013)

This modified DPSC is thermally more efficient in terms of air heating efficiency and the water heating efficiency has not declined significantly. This owes to the presence of porous media insert which increases the heat transfer area with air.

Building-integrated dual-function solar collector here proposed is able to provide passive space heating in cold winter, and water heating in warm seasons (Jie, 2011). In this study, evaluations were made on this modified collector system for the warm period operation under the water heating mode with natural circulation of flow. The results show that when working in the water heating mode, the system performs well in providing services hot water in the warm seasons without bringing in summer overheating problem.

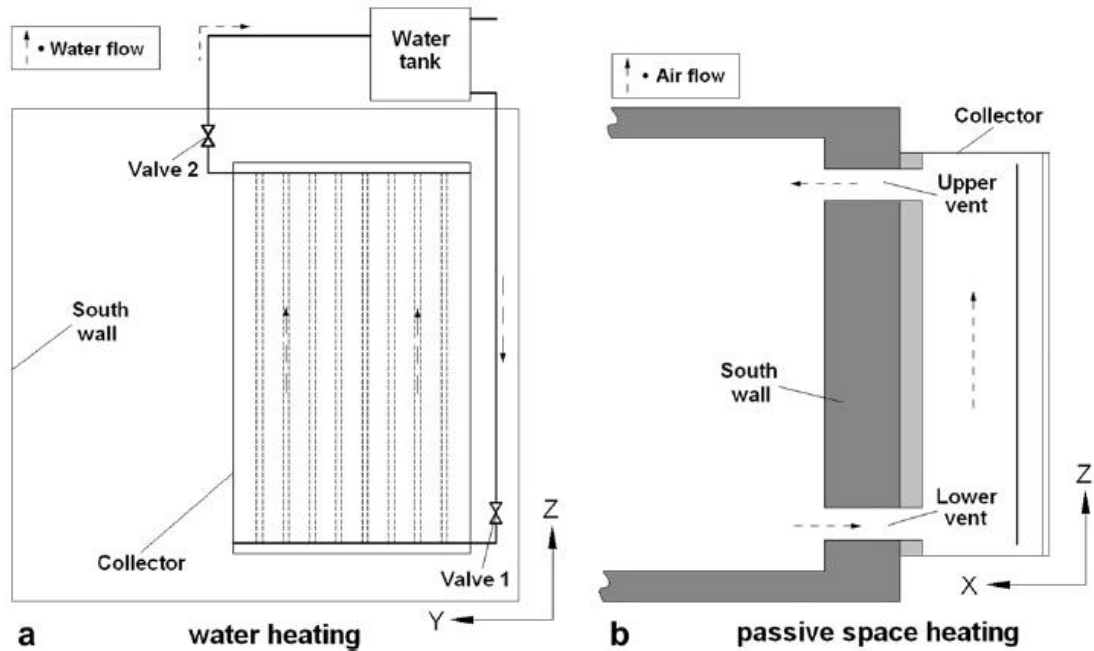


Figure 6 : Illustrative diagrams of the building-integrated dual-function solar collector system showing: (a) the water heating circuit and (b) the passive space heating (sectional view).

In energy and exergy analysis of DPSC (Jafari, 2011), the method of $\epsilon - NTU$ is used.

Analysis is performed for triangle channels. Parameters like the air flow rate and water inlet temperature are studied. Results are shown that DPSC has better energy and exergy efficiency than single collector. In addition, the triangle passage with water inlet temperature of 60°C has shown better exergy and energy efficiency. Results indicated that air section of DPSC increases heat delivery and efficiency of collector significantly at higher water inlet temperature. Exergy analysis indicated that air part can increase exergy efficiency of DPSC.

An experimental and theoretical investigation of dual purpose solar collector indicated that high temperature and high performance can be obtained using dual purpose solar collector (DPSC) compared to single water or air collector (Assari, 2009). A mathematical model based on effectiveness method has been developed for the investigation of thermal performance of DPSC. In the collector two fluids (water and air) flow simultaneously.

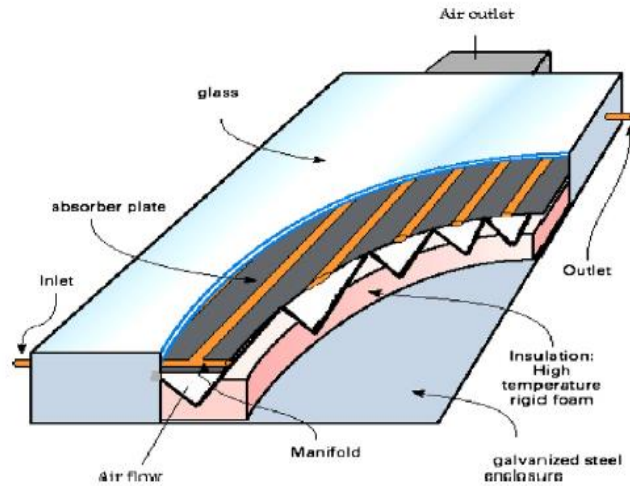


Figure 7 : Schematic of DPSC (Assari, 2009)

Three different kinds of channels were used to enhance the performance of collector, such as: rectangular fin, triangular fin and without fin.

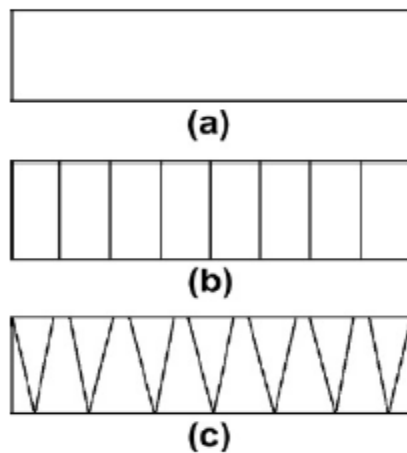


Figure 8 : Three kinds of air channels, (a) no fin, (b) with straight fin, (c) with triangular fin. (Assari, 2009)

It was concluded (Assari, 2009), in DPSC important parameters in heat delivery are: heat transfer coefficient between fluids, tubes and channels, heat transfer surface area, rate of fluids, fluid inlet temperature and solar radiation. The air section in DPSC absorbs a part of energy that water cannot deliver. In DPSC, like liquid collector heat delivery decreases with the increase of water inlet temperature whereas correspondingly heat delivery by air increases. Values of heat exchange effectiveness for straight fin are better than triangular fin. Hence, heat delivery in this situation is higher.

Experimental and theoretical study of the efficiency of a modified dual-function solar collector (Jinwei, 2011). The dual-function collector is modified from the conventional

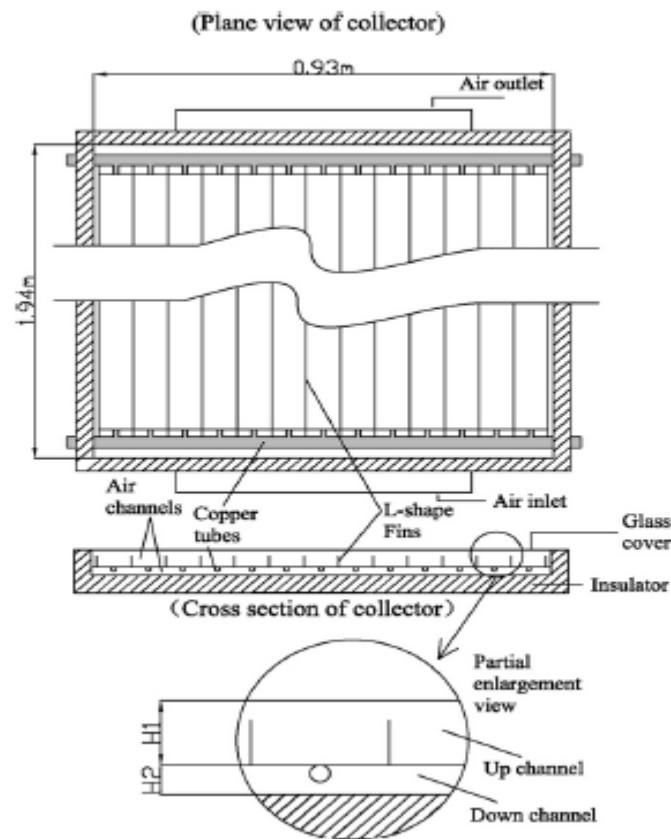


Figure 9 : Fig. The structure of the modified dual-function collector (Jinwei, 2011)

A copper tube is welded at the bottom of each L-shape aluminium fin. The fins of total 13 are arranged side by side within the gap between the cover glass and the back plate. Hence the gap is divided by the fins into up and down channels where the air flows through in the working mode of air heating, similarly as in a double-flow solar air collector.

The experiment results show that the collector can increase the temperature of 100 litre water by more than 30°C after absorbing solar radiation for a whole day. The daily efficiency in water heating mode reached 50 %. While in air heating mode, the daily mean and instantaneous efficiency reached 52 % and 55 %, respectively. The study shows that in air heating, although the efficiency increases with the flow rate, the temperature of the outlet air decreases with the flow rate. The L-shape fins in the dual-function collector have proved to have positive effect on the efficiency in air heating mode from the theoretic results.

2.3 Triple function photovoltaic/thermal solar collector

Photovoltaic/thermal (PV/T) solar collectors can provide electric power and thermal energy simultaneously. Either PV/T water collectors or PV/T air collectors can be left unused in some seasons because of the freezing problem of water and seasonal demand of hot air. Such kind of collectors have just been designed and very less research work has been published till now on these collectors.

In experimental investigation of tri-functional photovoltaic/thermal solar collector (Jie, 2014) a novel design of tri-functional PV/T solar collector was proposed. The collector can work in PV/water-heating mode or PV/air heating mode according to the seasonal requirements.

Experiments were conducted in different working modes under variable conditions to evaluate the performance of collector.

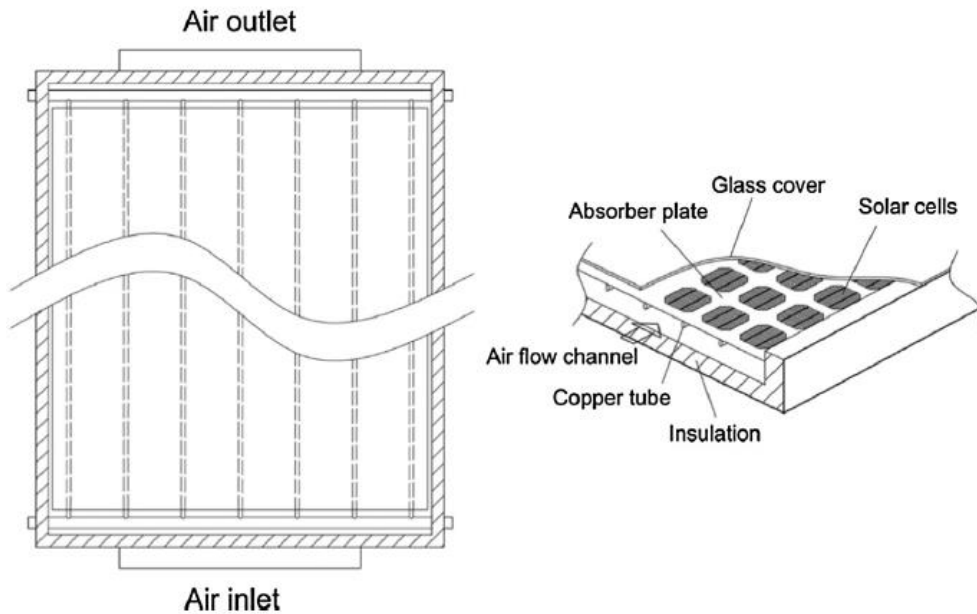


Figure 10 : Schematic of the tri-functional PV/T collector

The results show that the daily thermal efficiency achieved 46.0 % with the electrical efficiency of 10.2 % in PV/air-heating mode. The temperature increase of air reached 20°C with the flow rate of 0.033 kg/s on a sunny day. The instantaneously thermal efficiency at zero reduced temperature were 37.4 % and 44.3 % as the air flow rate was 0.026 kg/s and 0.032 kg/s respectively. In PV/water-heating mode, the thermal efficiency of the collector was 56.6 % at zero reduced temperature, and the daily thermal efficiency of the system was around 36.0 %. Compared with solar collectors presented by other authors, the tri-functional PV/T collector is able to operate efficiently in various conditions.

As a result of this literature survey, it was concluded that the hybrid collectors does hold an upper hand over the conventional solar collectors in many ways, with each kind of collector having its own advantages and disadvantages.

The air and water thermal collectors were much more cost efficient when compared to the thermal/PV collector or the triple function solar collectors and also the current conventional

solar collectors can be easily replaced with these dual-function solar collectors without making much changes to the installation setup. It also showed the ability to use dual-function solar collector to compensate for the heat losses by ventilation during the winter season. The performance of the air side of the model is significantly affected by the air channel shape, thus the focus was on improving the efficiency by changing the air flow pattern. So this research work is focused on introducing rectangular fins above the absorber plate.

3. CONCEPT FOR THE CURRENT DESIGN

The design for the dual function solar collector introduced in the thesis is similar to the fin tube heat exchanger. The idea here was to keep the collector price as low as possible by using the designs and components already available on the market. The model would be placed vertically with the air inlet being at the bottom and outlet at top. The water through the pipes would be horizontal passing through the fins.

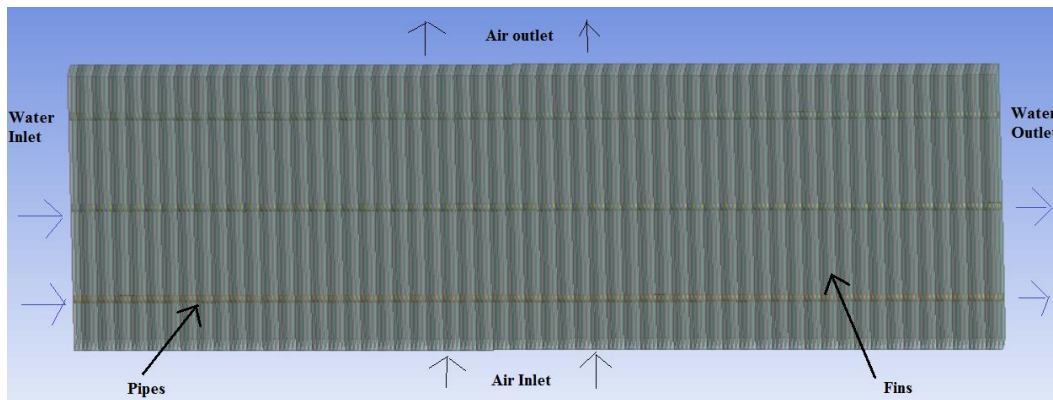


Figure 11 : Basic structure of collector

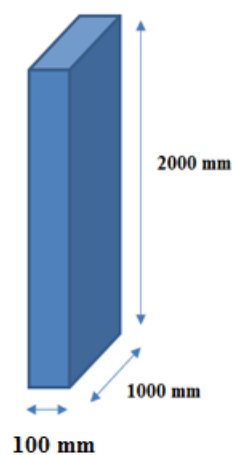


Figure 12 : Overall dimensions

The air flow and water flow were decided and inferred from the current designs in the market (Matuska, 2016). The overall dimensions were decided to be (2000 x 1000 x 40) mm.

Air flow: 80-160 m³/h. So in the model the average air flow of 120 m³/h was used.

Water flow: 40-100 l/h. In this model the average water flow of 70 l/h was used.

The model of fin tube heat exchanger by Lloyd coils was studied (www.lloydcoils.eu) and it was decided to keep the dimensions and the material of the proposed model similar to the already available ones.

Aluminium was selected for the fin material and Copper for pipes.

The fin height was kept constant at 40 mm and two geometries with fin spacing of 4.32 mm and 1.41 mm were constructed. The Copper pipes had dimensions of 7.94 x 0.28 mm and the spacing between the pipes was kept constant at 100 mm.

By performing the necessary calculations, a laminar flow of air through the gaps and also the flow of water through the pipes was observed.

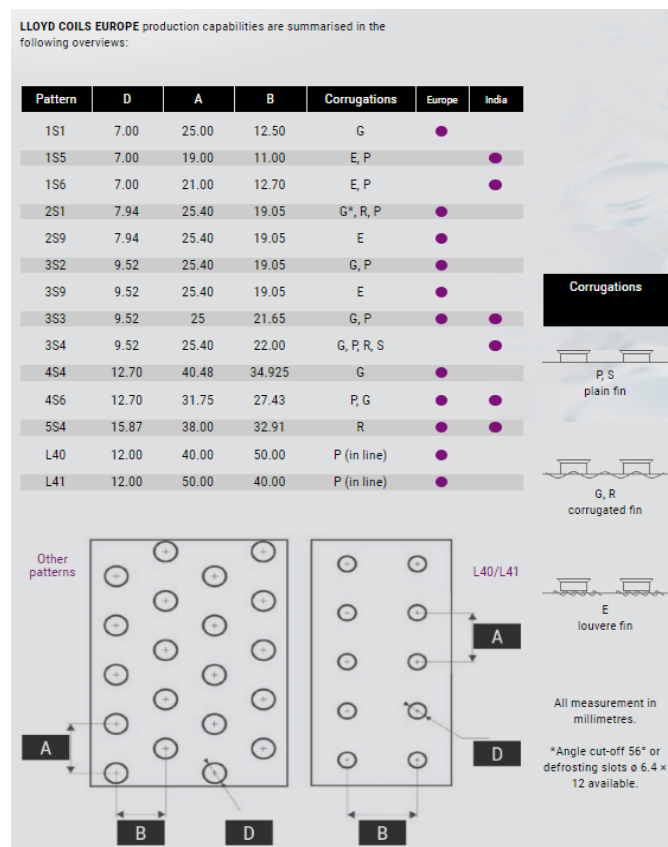


Figure 13 : Production capabilities by Lloyd coils (www.lloydcoils.eu)

3.1 Air inlet design

The model should have uniform air flow throughout the collector area, so to achieve that a slot diffuser had to be placed at the inlet side of the collector. For this purpose, TROX, VSD15 type slot diffuser was selected.

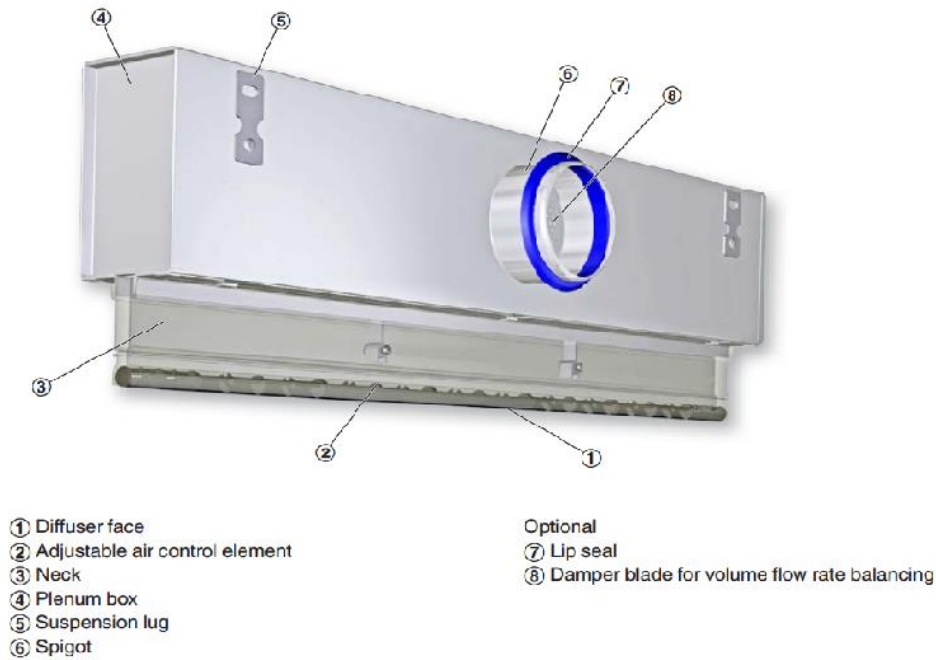


Figure 14 : Air inlet (slot diffuser) construction

- Nominal lengths from 600 to 1500 mm, 1 slot.
- Volume flow rate range 7 – 30 (l/s)/m or 25 – 108 (m³/h)/m.
- Diffuser face made of extruded aluminium sections.
- For variable and constant volume flows.
- Suitable for continuous linear arrangement.
- Individually adjustable air control elements to meet individual local requirements.

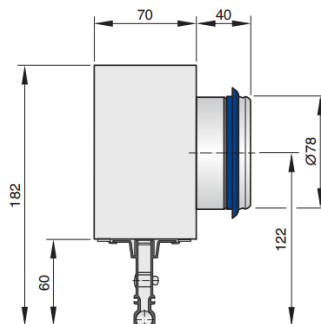


Figure 15 : Slot diffuser dimensions

As the width is 70 mm, it would fit in the inlet side of the air. The diffuser with 1 m nominal length is selected.

4. PRINCIPLES OF CFD

CFD techniques are used in many areas of engineering where fluid behaviour is the main element. Computational fluid dynamics (CFD) is concerned with the efficient numerical solution of the partial differential equations that describe fluid dynamics. Applied numerical analysis includes the solution of linear algebraic equations, ordinary and partial differential equations. Modelling of physical processes consist of the fluid flow and heat transfer. The use of general-purpose computer codes comprises commercial computational fluid dynamics software.

All CFD codes contain three main elements:

(1) A pre-processor which is used to input the problem geometry, generate the grid and define the flow parameters and the boundary conditions to the code.

(2) A flow solver which is used to solve the governing equations of the flow subject to the conditions provided. There are four different methods used as a flow solver:

(i) Finite difference method

(ii) Finite element method

(iii) Finite volume method

(iv) The spectral method.

(3) A post-processor which is used to display the data and show the results in graphical and easy to read format.

For the finite-volume approach the integral form of the governing equations of heat and mass transfer processes are applied to the control volume of the cells, which make up the discretizational (computational) model of a continuous physical domain of the specific physical system under investigations. Normally the value at the centre of a cell is stored and the values at the faces are interpolated to give the values across the boundaries. It is also possible to obtain similar equations for the conservation of momentum and energy for each cell. From these equations it is then possible to create a set of simultaneous equations where either the value in the cell is equal to a boundary condition and/or a combination of the properties according to the discrete equations. Eventually, there would be a number of simultaneous equations equal to the number of independent discrete variables. These can be represented as a large matrix of algebraic equations which the computer then solves.

4.1 Flow Calculation

The flow is governed by the continuity equation, the energy equation and Navier-Stokes momentum equations. Transport of mass, energy and momentum occur through convective flow and diffusion of molecules and turbulent eddies.

The momentum balance, also known as the Navier-Stokes equations, follows Newton's second law: The change in momentum in all directions equals the sum of forces acting in those directions. There are two different kinds of forces acting on a finite volume element, surface forces and body forces. Surface forces include pressure and viscous forces and body forces include gravity, centrifugal and electro-magnetic forces.

The continuity equation is difficult to solve numerically. In CFD programs, the continuity equation is often combined with momentum equation to form Poisson equation.

Energy is present in many forms in flow i.e. as kinetic energy due to the mass and velocity of the fluid, as thermal energy, and as chemically bounded energy. Thus the total energy can be defined as the sum of all these energies.

The coupling between energy equations and momentum equations is very weak for incompressible flows, thus equations for kinetic and thermal energies can be written separately. The chemical energy is not included because there was no species transport involved in this project.

4.2 Radiation model

In the model Radiation surface to surface (S2S) model has been used. ANSYS FLUENT's S2S radiation model assumes the surfaces to be grey and diffuse. Heat radiation is the process by which energy, in the form of electromagnetic radiation, is emitted by a heated surface in all directions and travels directly to its point of absorption at the speed of light; thermal radiation does not require an intervening medium to carry it.

Emissivity and absorptivity of a grey surface are independent of the wavelength. Also, by Kirchhoff's law, the emissivity equals the absorptivity ($\epsilon = \alpha$). For a diffuse surface, the reflectivity is independent of the outgoing (or incoming) directions.

Also, as stated earlier, for applications of interest, the exchange of radiative energy between surfaces is virtually unaffected by the medium that separates them. Thus, according to the grey-body model, if a certain amount of radiant energy (E) is incident on a surface, a fraction (ΨE) is reflected, a fraction (αE) is absorbed, and a fraction (τE) is transmitted. Since for most applications the surfaces in question are opaque to thermal radiation (in the infrared spectrum), the surfaces can be considered opaque. The transmissivity, therefore, can be

neglected. It follows, from the conservation of energy, that $\alpha + \Psi = 1$, since $\alpha = \epsilon$ (emissivity), and $\Psi = 1 - \epsilon$.

4.3 Solar Load Model

ANSYS FLUENT provides a solar load model that can be used to calculate radiation effects from the sun's rays that enter a computational domain. The ray tracing approach is a highly efficient and practical means of applying solar loads as heat sources in the energy equations. It includes a solar calculator utility that can be used to construct the sun's location in the sky for a given time-of-day, date, and position. Solar load is available in the 3D solver only, and can be used to model steady and unsteady flows. It will allow the solar transmission through all glazed surfaces to be determined over the course of a day, allowing important decisions to be made before undertaking any flow studies.

The solar load model's ray tracing algorithm can be used to predict the direct illumination energy source that results from incident solar radiation. It takes a beam that is modelled using the sun position vector and illumination parameters, applies it to any or all wall or inlet/outlet boundary zones that you specify, performs a face-by-face shading analysis to determine well-defined shadows on all boundary faces and interior walls, and computes the heat flux on the boundary faces that results from the incident radiation.

The resulting heat flux that is computed by the solar ray tracing algorithm is coupled to the ANSYS FLUENT calculation via a source term in the energy equation. The sun position vector and solar intensity is computed from the solar calculator. Direct and diffuse irradiation parameters can also be specified using a user-defined function.

Solar ray tracing presents less computational overhead than discrete ordinates, as it calculates the solar loads once at the beginning of a steady-state simulation. However, it uses some

simplifying assumptions to do so. It does not calculate the emission from surfaces, and the reflecting component of the incident load is distributed uniformly across all participating surfaces rather than retained locally at the surfaces reflected to.

4.4 Solar Calculator

ANSYS FLUENT provides a solar calculator that can be used to compute solar beam direction and irradiation for a given time, date, and position. These values can be used as inputs to the solar ray tracing algorithm or as semi-transparent wall boundary.

Inputs/Outputs

Inputs needed for the solar calculator are:

- global position (latitude, longitude, time zone)
- starting date and time
- mesh orientation
- solar irradiation method
- sunshine factor

The following values are computed by the solar calculator and are displayed in the console whenever the solar calculator is used:

- sun direction vector
- sunshine fraction
- direct normal solar irradiation at earth's surface
- diffuse solar irradiation - vertical and horizontal surface
- ground reflected (diffuse) solar irradiation - vertical surface

5. MANUAL CALCULATIONS

This chapter deals with the calculation of radiation heat transfer losses in the collector and the pressure losses which occurs along the fins. A pattern was derived showing the dependency of radiation losses and pressure losses on the spacing between the fins.

5.1 Heat loss by Radiation

The focus was on a single channel, enclosed system with fins on two side and with glass at top and the absorber plate at the bottom.

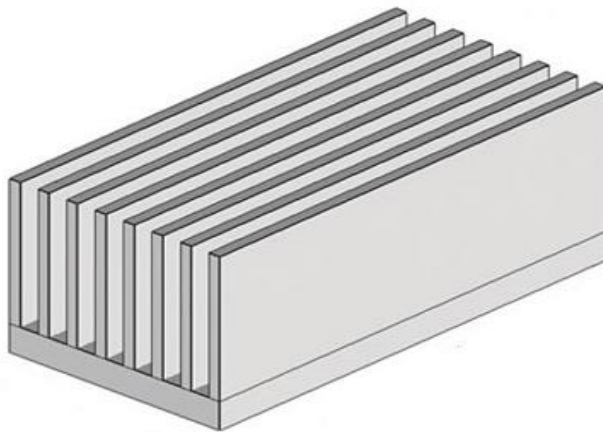


Figure 16 : The structure of the modified dual-function collector with absorber plate at bottom and rectangular fins. (www.electronics-cooling.com)

Only one single channel of the rectangular fins was taken into consideration. The radiation losses through this one channel was calculated. In the radiation analysis of an enclosure, either the temperature or the net rate of heat transfer has to be given for each of the surfaces to obtain a unique solution for the parameters of the enclosure. In this method we have taken into account the temperatures of all the surfaces in the enclosure.

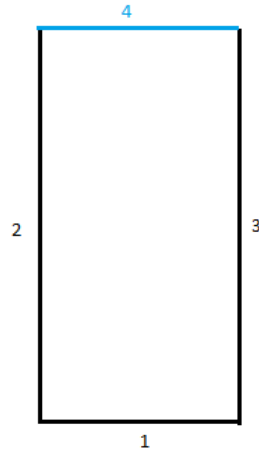


Figure 17 : The 2-D structure of a single channel

$$\sigma T_i^4 = J_i + \frac{1-\varepsilon_i}{\varepsilon_i} \left(\sum_{j=1}^N F_{i-j} (J_i - J_j) \right) \quad (5.1)$$

σ – Stefan Boltzmann constant ($5.670367 \times 10^{-8} \text{ W m}^{-2} \text{ K}^{-4}$)

T_i - Surface temperatures (K)

J_i – Radiosities (W/m^2)

ε – Emissivity (-)

F_{i-j} – View factor (-)

In this figure the surface 1 is the absorber plate and surfaces 2 and 3 are the rectangular fins. The surface 4 is the glass top. There is a very small air gap between the glass top (4) and the fin structure (2 and 3). This air gap can be neglected and the system can be considered to be an enclosed system of surfaces.

To use the equation (1), we need to know the view factor F_{i-j} of all the four surfaces towards each other.

Surfaces 1 and 2 are long plates of unequal widths and with one common edge and at an angle of 90° to each other.

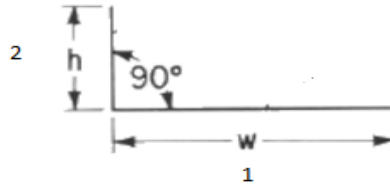


Figure 18 : Surfaces 1 and 2 with a common edge

The view factor of surface 1 to surface 2 is F_{1-2}

$$F_{1-2} = \frac{1}{2} \left(1 + \frac{h}{w} - \sqrt{1 + \left(\frac{h}{w}\right)^2} \right) \quad (5.2)$$

Here we have the height of the fins as constant which is 40 mm.

The conservation of energy principle states that the entire radiation leaving any surface i of an enclosure be intercepted by the surfaces of the enclosure. Therefore, the sum of the view factors from surface i of an enclosure to all surfaces of the enclosure, including to itself, must equal unity. This is called summation rule for an enclosure and is expressed as

$$\sum_{j=1}^N F_{i-j} = 1 \quad (5.3)$$

So in this case,

$$F_{1-1} + F_{1-2} + F_{1-3} + F_{1-4} = 1 \quad (5.4)$$

Here, $F_{1-1} = 0$ as the surface is plane. And the enclosure is symmetrical, we also know that $F_{1-2} = F_{1-3}$. Thus

$$F_{1-4} = 1 - (F_{1-2} + F_{1-3}) \quad (5.5)$$

From this relation we can find the dependency of F_{1-4} on the width (w) i.e the gap between the two fins.

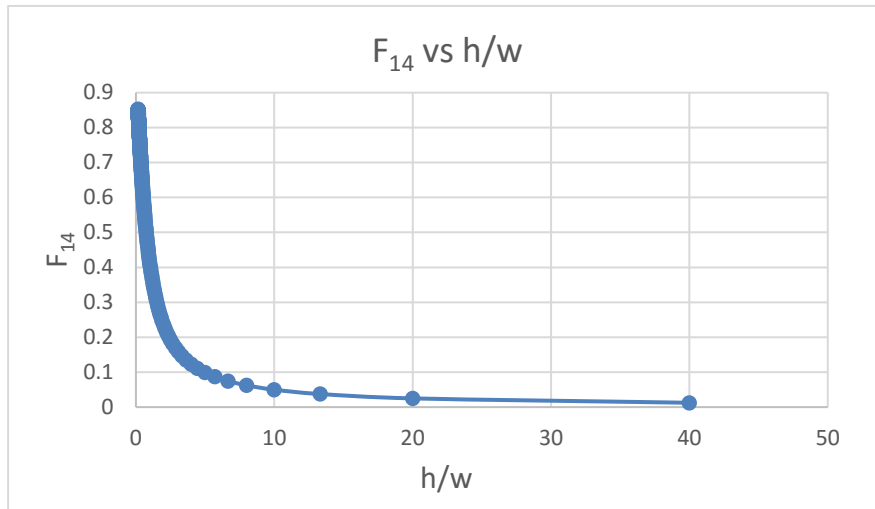


Figure 19 : F₁₄ vs h/w

In this case we have kept the height of the fins constant to 40mm.

To use equation (5.1) we also need to calculate the view factor for surface 2 to surface 4.



Figure 20 : The surfaces 2 and 3.

$$F_{2-3} = \sqrt{1 + \left(\frac{w}{h}\right)^2} - \frac{w}{h} \quad (5.6)$$

As we have decided to keep the height of the rectangular fins constant, we just keep varying the width between the fins from 0.5 mm to 20 mm.

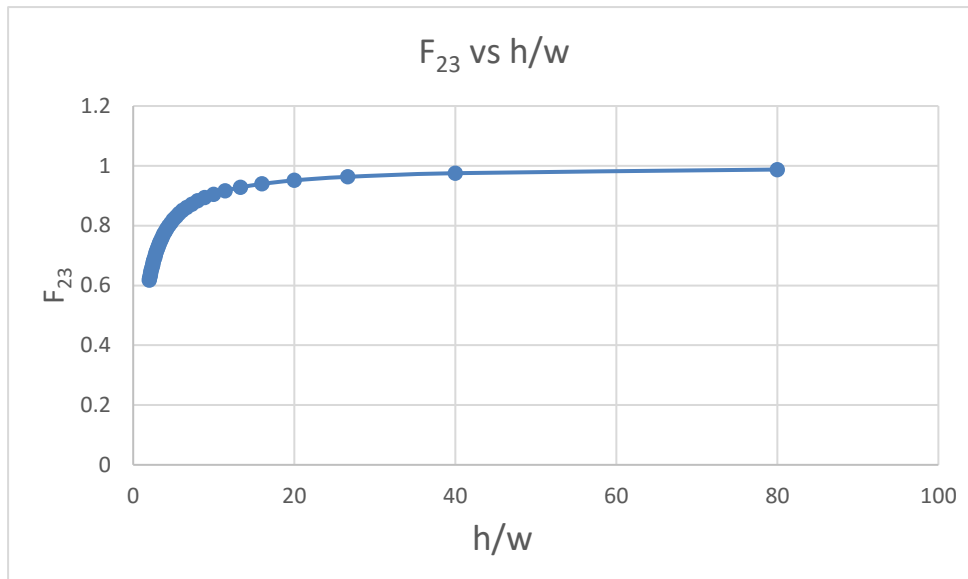


Figure 21 : Graph for F23 vs h/w

Again to use equation (5.1), we need to know the view factor of all the surfaces and from the above calculations we know F_{2-3} and F_{1-4} . As these four surfaces form a closed system and is symmetrical about the vertical and horizontal axis. So we can come to these relations

$$F_{1-2} = F_{1-3} = F_{4-2} = F_{4-3} \quad (5.7a)$$

$$F_{1-4} = F_{4-1} \quad (5.7b)$$

$$F_{2-1} = F_{3-1} = F_{2-4} = F_{3-4} \quad (5.7c)$$

$$F_{2-3} = F_{3-2} \quad (5.7d)$$

$$F_{2-4} = F_{3-4} \quad (5.7e)$$

Now we have all the requirements to find the amount of radiation leaving the channel from the top surface. For this calculation, the emissivities of the surfaces were taken as, surfaces 1, 2 and 3 are all made from aluminium with $\epsilon_1 = \epsilon_2 = \epsilon_3 = 0.1$ and the emissivity of top surface is $\epsilon = 0.9$. From this we form the system of equations,

$$\sigma T_i^4 = J_i + \frac{1-\varepsilon_i}{\varepsilon_i} (\sum_{j=1}^N F_{i-j} (J_i - J_j)) \quad (5.8a)$$

$$\sigma T_1^4 = J_1 + \frac{1-\varepsilon_1}{\varepsilon_1} (F_{12}(J_1 - J_2) + F_{13}(J_1 - J_3) + F_{14}(J_1 - J_4)) \quad (5.8b)$$

$$\sigma T_2^4 = J_2 + \frac{1-\varepsilon_2}{\varepsilon_2} (F_{21}(J_2 - J_1) + F_{23}(J_2 - J_3) + F_{24}(J_2 - J_4)) \quad (5.8c)$$

$$\sigma T_3^4 = J_3 + \frac{1-\varepsilon_3}{\varepsilon_3} (F_{31}(J_3 - J_1) + F_{32}(J_3 - J_2) + F_{34}(J_3 - J_4)) \quad (5.8d)$$

$$\sigma T_4^4 = J_4 + \frac{1-\varepsilon_4}{\varepsilon_4} (F_{41}(J_4 - J_1) + F_{42}(J_4 - J_2) + F_{43}(J_4 - J_3)) \quad (5.8e)$$

We have four unknown radiosities (J), so we use the matrix method to find out the four values. After obtaining the four radiosities, the system is represented using the circuit diagram below

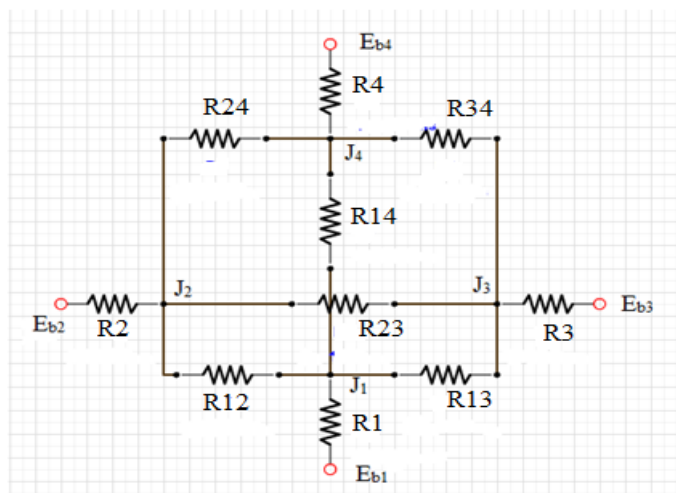


Figure 22 : Heat radiation circuit.

In the above diagram we know the value of all the resistances,

$$R1 = \frac{1-\varepsilon_1}{A_1\varepsilon_1}, \quad R2 = \frac{1-\varepsilon_2}{A_2\varepsilon_2}, \quad R3 = \frac{1-\varepsilon_3}{A_3\varepsilon_3}, \quad R4 = \frac{1-\varepsilon_4}{A_4\varepsilon_4} \quad (5.9a)$$

$$R12 = \frac{1}{A_1F_{12}}, \quad R13 = \frac{1}{A_1F_{13}}, \quad R14 = \frac{1}{A_1F_{14}} \quad (5.9b)$$

$$R24 = \frac{1}{A_2F_{24}}, \quad R23 = \frac{1}{A_2F_{23}} \quad (5.9c)$$

$$R34 = \frac{1}{A_3F_{34}} \quad (5.9d)$$

Using these resistances and the radiosity values we can find the amount of heat being removed from one channel through the top surface, thus we can find out the total heat being lost by radiation from the collector.

5.2 Pressure loss across the collector

In this section the pressure loss along the solar collector fins has been calculated. A slot diffuser was used on one side of the collector to have an even flow throughout the collector. The method presented here has been explained in the electronics cooling magazine. This method assumes that the air flow rate is given, either in terms of the average velocity, V , between the fins or a volumetric flow rate, G .

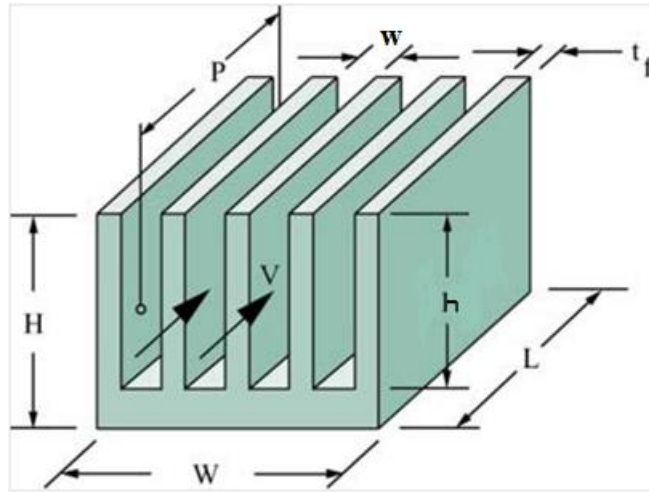


Figure 23 : Rectangular Fin structure

The pressure drop across the heat sink ΔP , is given by

$$\Delta P = (K_c + 4 \cdot f_{app} \cdot \frac{L}{D_h} + K_e) \cdot \rho \cdot \frac{V^2}{2} \quad (5.10)$$

All the variables in the above equation are explained below

The hydraulic diameter, D_h , is approximately equal to $(2 \times w)$ where w is the gap between the fins given by

$$w = \frac{W - N_{fin} \cdot t_f}{N_{fin} - 1} \quad (5.11)$$

The coefficients K_c and K_e represent the pressure losses due to the sudden contraction and expansion of the flow entering and leaving the flow channels between the fins. These coefficients may be determined using

$$K_c = 0.42 \cdot (1 - \Omega^2) \quad (5.12)$$

$$K_e = (1 - \Omega^2)^2 \quad (5.13)$$

$$\Omega = 1 - \frac{t_f \cdot N_{fin}}{W} \quad (5.14)$$

The average velocity for use in the main equation is related to the volumetric air flow rate, by

$$V = \frac{G}{N_{fin} \cdot w \cdot h} \quad (5.15)$$

The apparent friction factor, for hydro dynamically developing laminar flow is related to the friction factor, f , and may be calculated from

$$f_{app} = \frac{[\left(\frac{3.44}{\sqrt{L^*}}\right)^2 + (f \cdot Re)^2]^{1/2}}{Re} \quad (5.16)$$

Where L^* is given by

$$L^* = \frac{L/D_h}{Re} \quad (5.17)$$

and the Reynolds number, Re , is given by

$$Re = \frac{\rho \cdot V \cdot D_h}{\mu} \quad (5.18)$$

The friction factor for fully developed laminar flow used in Equation (5.16) is a function of both the aspect ratio $\lambda = (w/h)$, of the heat sink flow channels and the Reynolds number as given by

$$f = (24 - 32.527 \cdot \lambda + 46.271 \cdot \lambda^2 - 40.829 \cdot \lambda^3 + 22.954 \cdot \lambda^4 - 6.089 \cdot \lambda^5) / Re \quad (5.19)$$

6. CFD MODEL

This section describes the CFD process for this investigation. There were investigated two models of the collector, in the first one the air side of the collector and in the second one the water side of the collector was simulated. The first two subchapters (Sections 6.1 and 6.2) cover geometry and meshing process and the final subchapter (Section 6.3) covers the boundary conditions for the model.

6.1 Modelling

A section of the collector geometry is made in the design modeller.

6.1.1 Air side geometry

To simulate the air side of the collector, full length of the air flow was designed to study the entire air flow pattern, which is 2m (entire length of a fin) while along the breadth the small section that is 5 fins were drawn. As the geometry of the fins is repetitive, we have considered only 5 fins with the outer two fins imagined as the outer boundary of the collector.

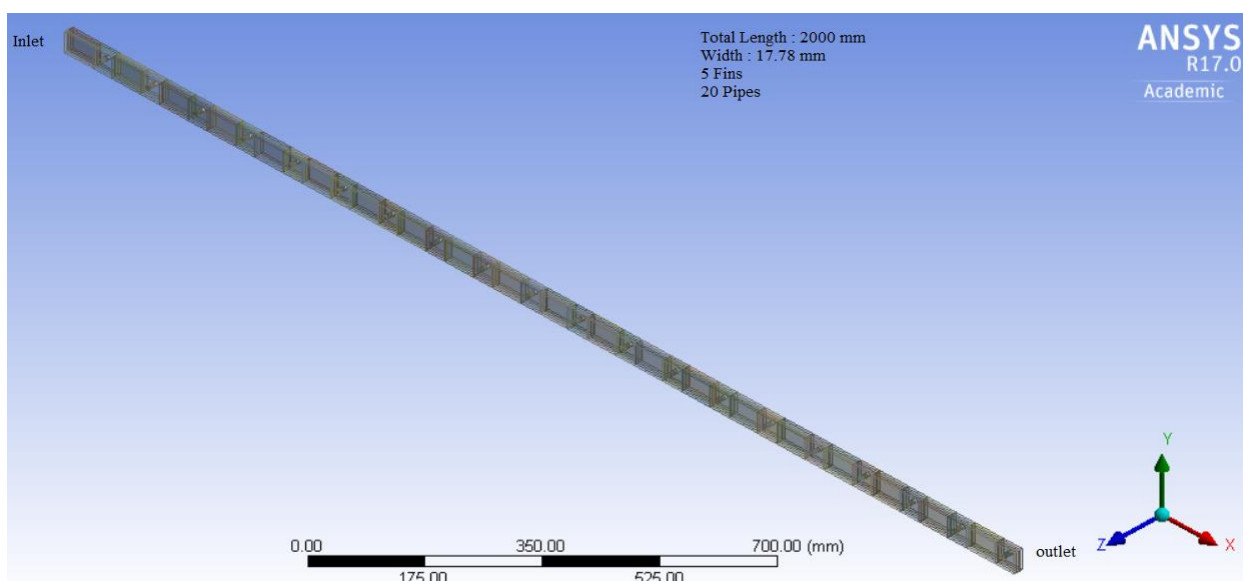


Figure 24: Collector with wide gap (4.32 mm)

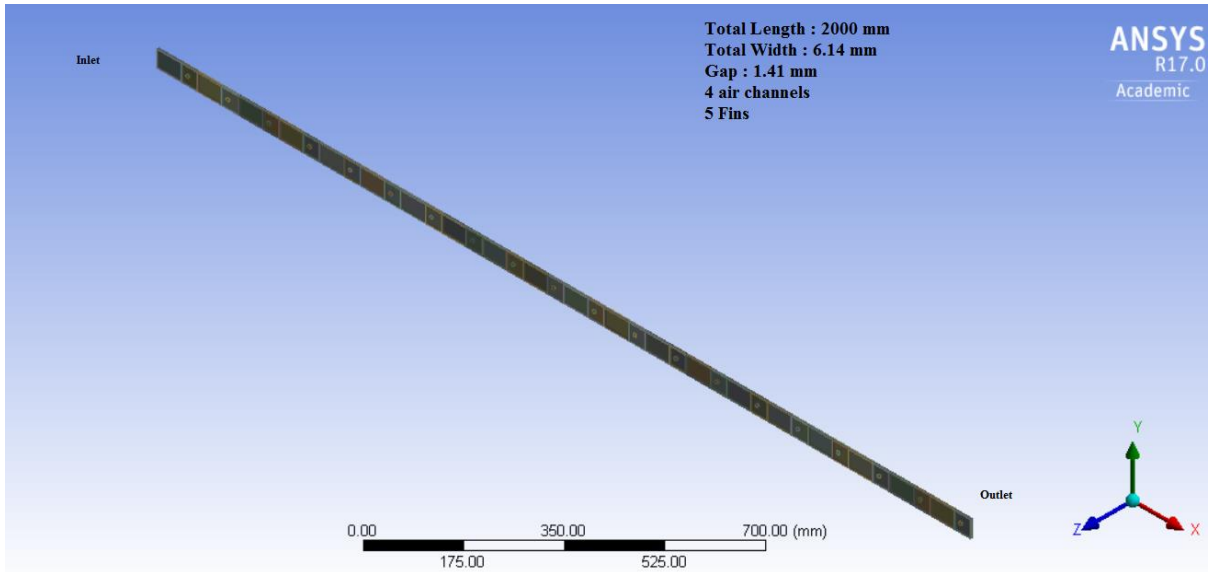


Figure 25 : Collector with narrow gap (1.41 mm)

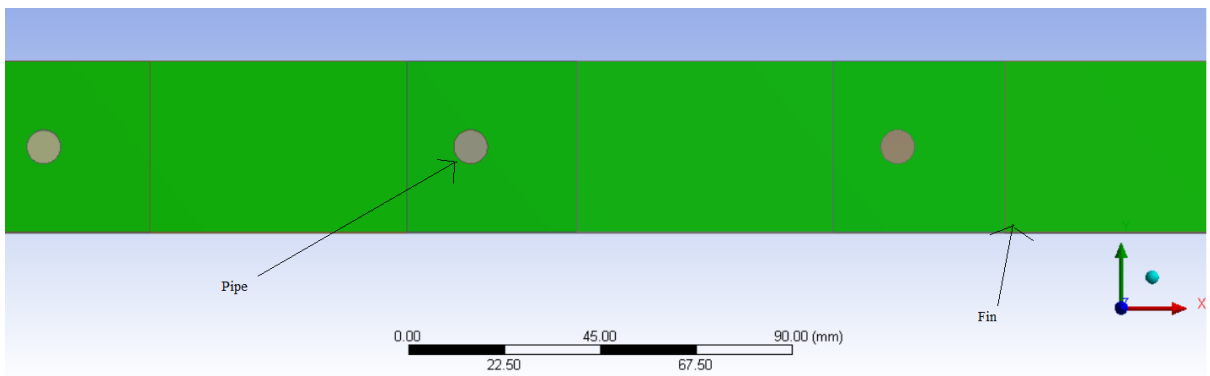


Figure 26 : Front View of the fins and the pipe (both collector)

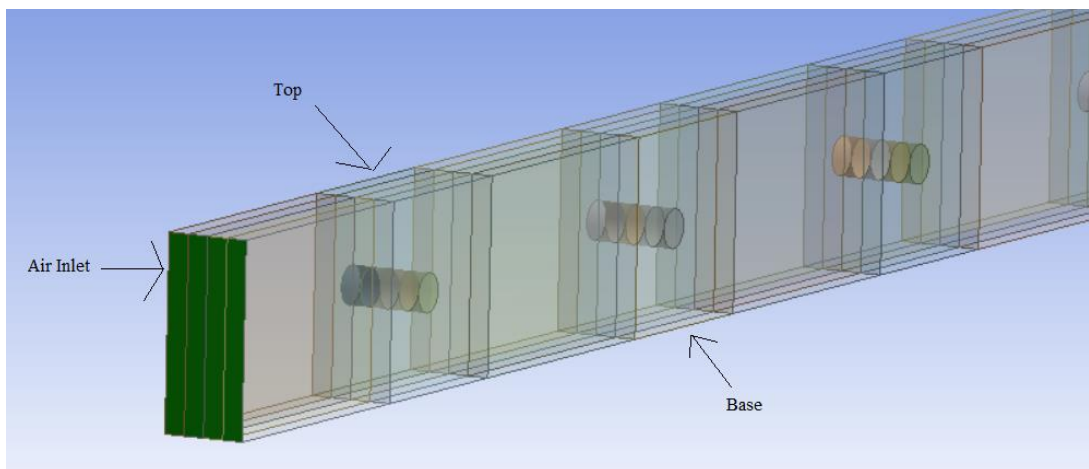


Figure 27 : Detail View of the inlet, top glass cover and base absorber plate.

Table 6.1: Solar Collector geometry details for air side

	Wide Gap (4.32 mm)	Narrow Gap (1.41 mm)
Total Length	2000 mm	1000 mm
Total Width	17.78 mm	300 mm
Pipe Diameter	7.94 x 0.28 mm	7.94 x 0.28 mm
Fin Thickness	0.1 mm	0.1 mm
No. fins	5	5
No. of air channels	4	4
No. of pipes	20	20

6.1.2 Water Side Geometry

For simulating the water side of the collector, the entire flow of the water was designed i.e. the full geometry of 3 pipes. So it includes all the fins.

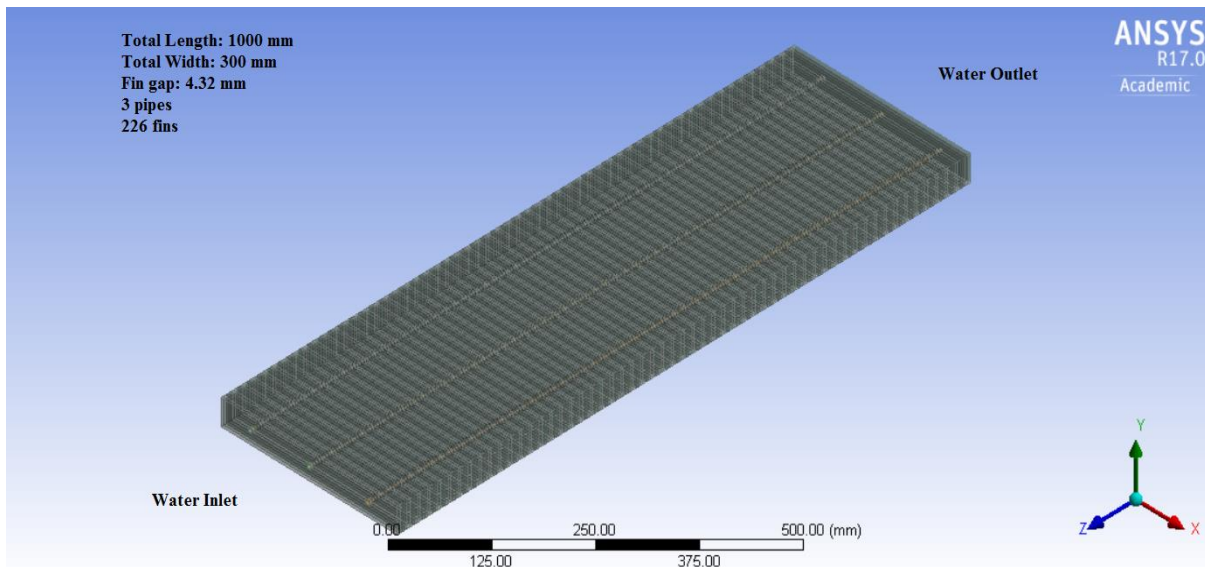


Figure 28 : Collector with wide gap

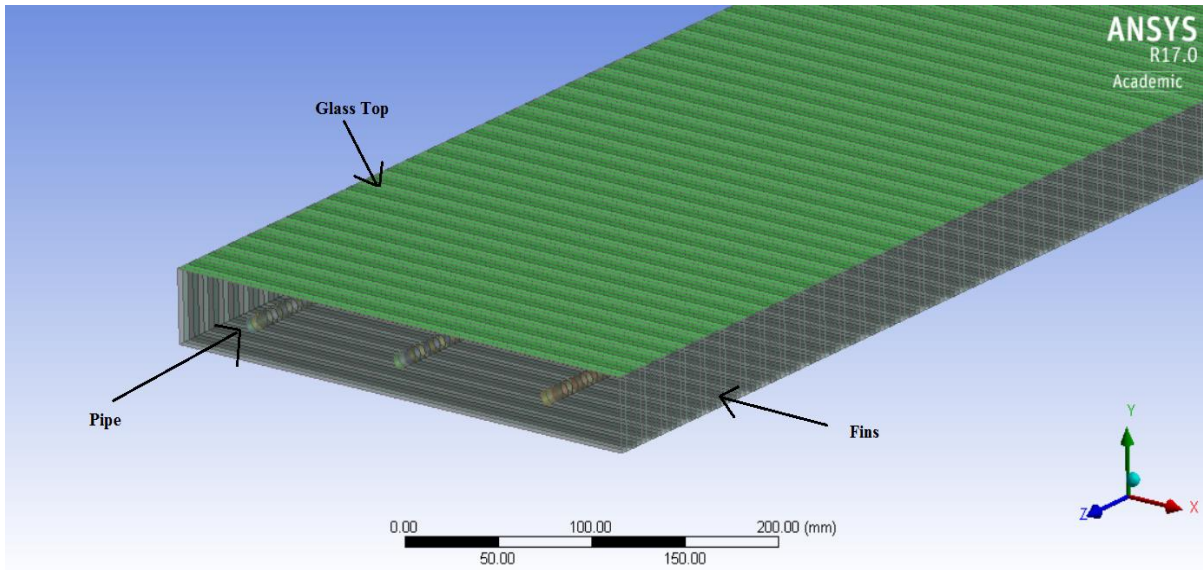


Figure 29 : Inlet, Glass top and Fins of collector.

Table 6.2 Solar Collector geometry details for water side

	Wide Gap (4.32 mm)	Narrow Gap (1.41 mm)
Total Length	1000	1000
Total Width	300	300
Pipe Diameter:	7.94 x 0.28	7.94 x 0.28
Fin Thickness	0.1 mm	0.1 mm
No. fins:	662	226
No. of air channels:	661	225
No. of pipes	3	3

6.2 Meshing

A hexahedral mesh was created in all the models. Hex (or quad) meshes generally work better (i.e., more accurate) for wall-bounded flows since we can maintain orthogonal grids in the wall-normal direction. This is a consequence of the better accuracy of the hex elements since the angle between faces can be kept close to 90-degrees.

Aside from "numerical" efficiency, there is also a "computational" efficiency factor. Structured grids with hex or quad meshes (either regular or curvilinear) can be implemented a bit easier and usually execute quite a bit faster than algorithms that support unstructured (usually with tets but can be a blend of tets, prisms, and hexs). This is because of the implicit topology of the structured grid.

6.2.1 Meshing for air side model

In the air model meshing we have achieved a very fine mesh around the pipes as the air flow would become complicated around the pipes and in the area between the pipes the air flow would again develop a laminar flow. So we have kept the hex mesh coarse and long.

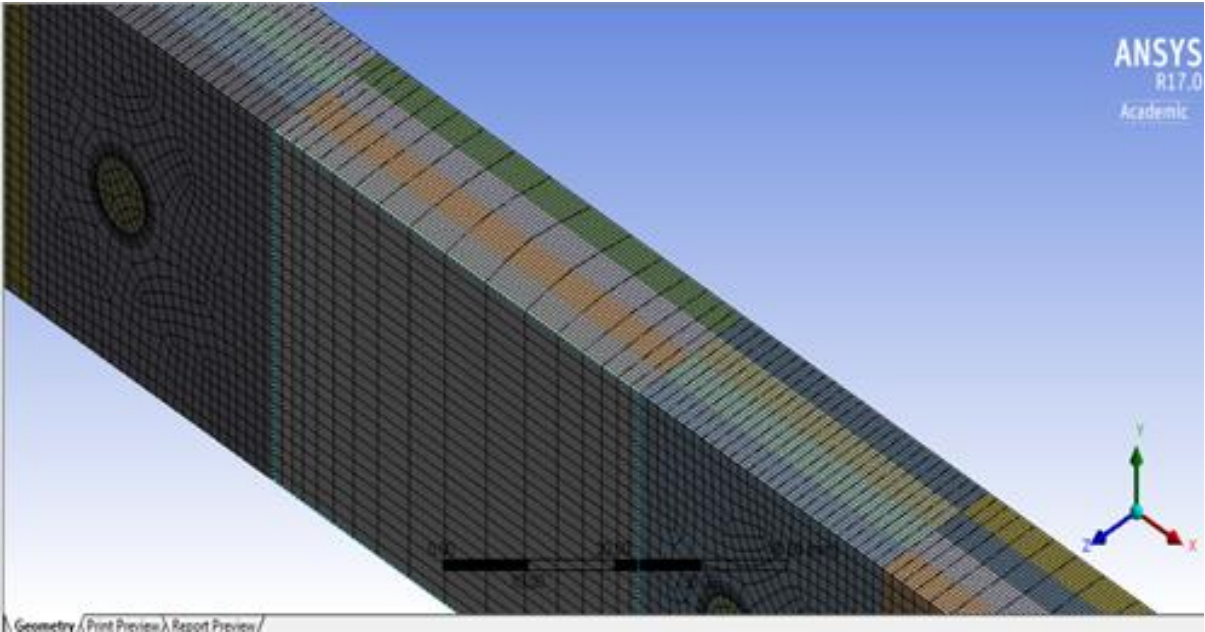


Figure 30 : Meshing details of air side model.

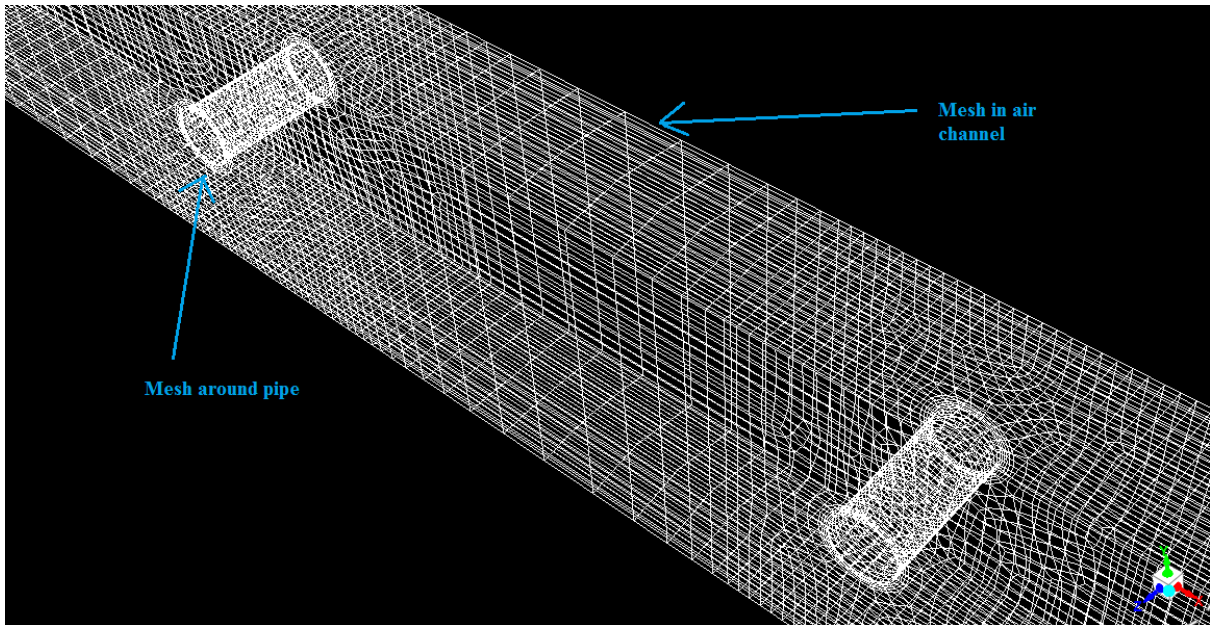


Figure 31 : Mesh model in Fluent.

A similar mesh model was made for both the air side model with fin gaps 4.32 mm and 1.41 mm.

Table 6.3 Mesh Details for air side geometry

	Wide gap (4.32 mm)	Narrow gap (1.41 mm)
Nodes	871596	815744
Elements	596791	550284

6.2.2 Meshing for water model

In this model, the main focus was to analyse the flow of water in the pipes and the air flow between the gaps was secondary. So a fine mesh was made inside the pipes and a coarser mesh was made between the fins.

Table 6.4 Mesh Details for water side geometry

	Wide gap (4.32 mm)	Narrow gap (1.41 mm)
Nodes	1360593	1830544
Elements	1322100	1804411

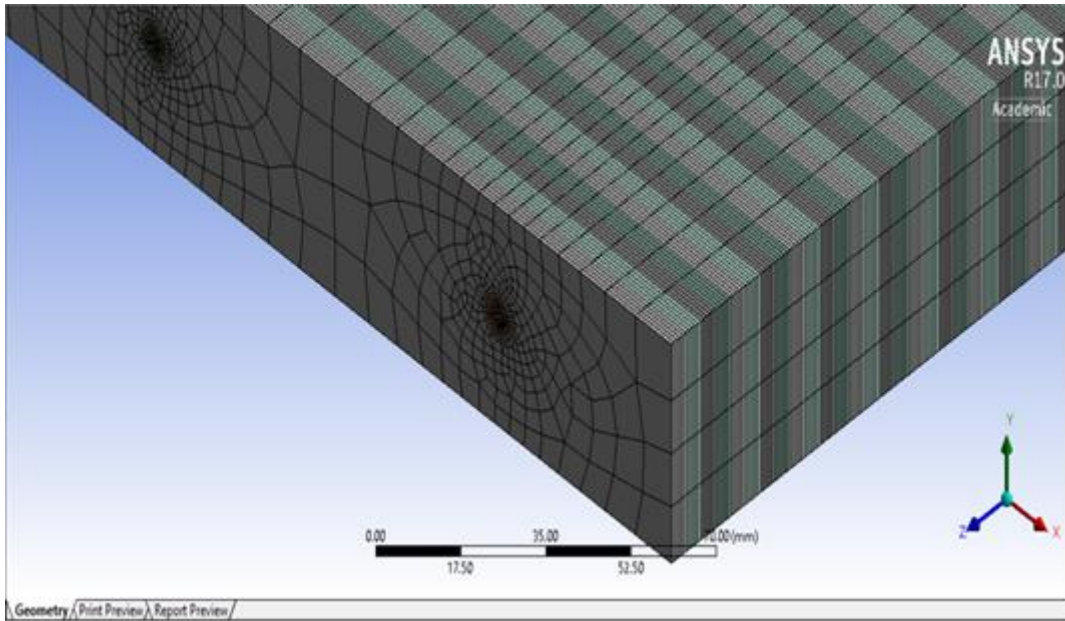


Figure 32 : Mesh Model for water side model

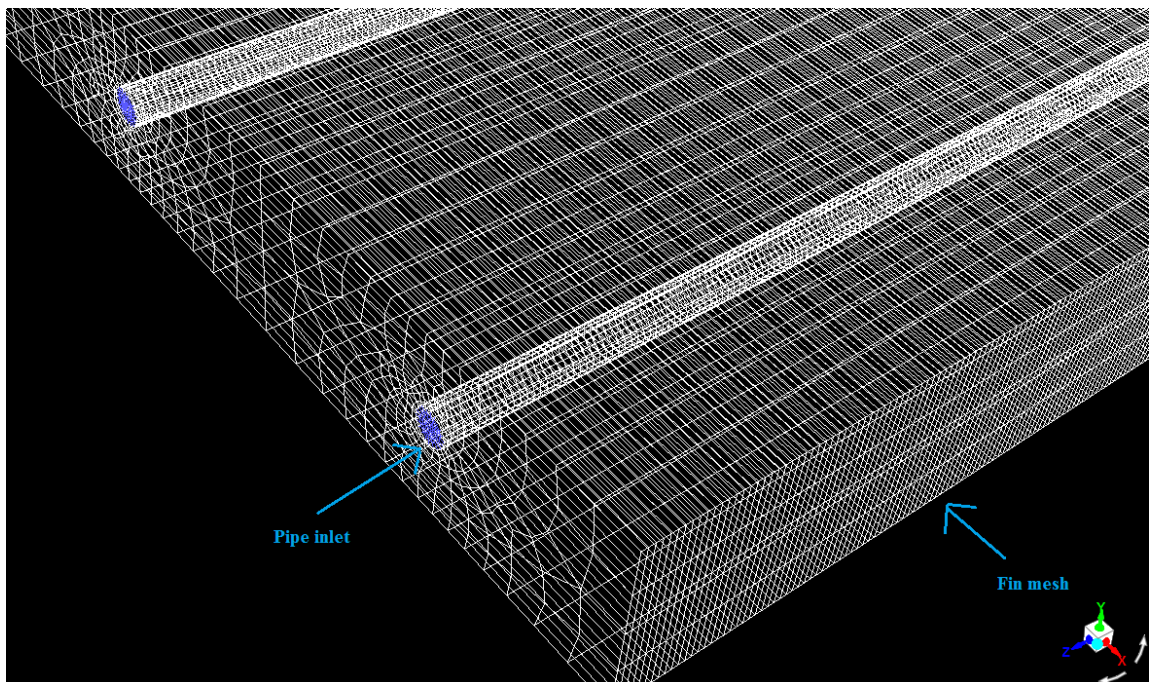


Figure 33 : Mesh Model in Fluent.

6.3 Boundary Conditions

As 4 models had been created

- Air model with 4.32 mm fin gap
Air model with 1.41 mm fin gap
- Water model with 4.32 fin gap
Water model with 1.41 mm gap.

6.3.1 Air side model boundary conditions

For all the air models,

- The volumetric air flow is between 80-160 m³/h. The average value of 120 m³/h was taken for calculation.
- The velocity of air in each gap was found out to be 0.853545 m/s for wide gap collector and 0.8927742 m/s for narrow gap collector.
- The base of the collector was considered as adiabatic and was taking part in shell conduction. The thickness was 0.5 mm and it took part in the solar ray tracing and also in the view factor calculation.
- The outer two fins were assigned the properties like the exterior of the collector, they were adiabatic and also participated in the solar ray tracing and view factor calculation.
- The interior fins had fluid region on both the sides, so it was assigned as a two sided wall and the coupled thermal boundary condition was applied. It also took part in solar ray tracing and view factor calculation.
- Inlet was velocity inlet.
- Outlet was pressure outlet.
- The pipe wall was also coupled as it had fluid region on both the sides.
- The glass cover of the surface was taking part in convection and radiation both so it was assigned mixed thermal boundary condition.

1. The heat transfer coefficient was calculated using the Mc Adams formula

$$H_c = 5.3 + 3.6*v \quad (v \text{ is the wind velocity in m/s.})$$

2. Free Stream Temperature is the external air temperature.
3. External Radiation Temperature was the average temperature of the air and the effective sky temperature.
4. The glass properties of absorptivity, transmissivity and internal and external emissivity were selected using the “BERKELEY LAB WINDOW v7.4.8.0 Glazing System Thermal and Optical Properties”
5. As the water flow would be stopped, it was assumed as solid type of material with water thermal properties inside the pipes.
6. The shell conduction was enabled for the wall type boundary conditions. If shell conduction is enabled, the shell cell temperature will be stored in the "inner" surface. If there is no shell conduction, then the "outer" surface stores the face temperature of the wall while the "inner" surface stores the evaluated value of the boundary condition specified by the user.

6.3.2 Water side model

For all the water model

- The water flow rate was between 40-100 m³/h. So the average of 70m³/h was taken into calculation.
- The velocity of 0.0257 m/s was calculated inside the pipes.

All the boundary conditions were taken as same for the air model. Here the only difference was the water was not assumed to be solid and its flow inside the pipe was calculated.

All the models were simulated with selective and non-selective coatings.

For Non-selective coating, the emissivity for the absorber plate, fins and pipe surface were taken as 0.9.

For surfaces with selective coating of the surfaces, the internal emissivity was 0.1 and the $\alpha_{\text{vis}}=0.9$ (absorptivity for direct visible) and $\alpha_{\text{ir}} = 0.1$ (absorptivity for infrared) was assumed.

As the models were simulated for two days of the year, 21-June and 21-December and for every hour from 0900 to 1600 hours. The following data for Praha-Ruzyne was taken.

Location: N 50° 06' E 14° 17'

Date: 21-12-2015

Table 6.4 Climate data for winter

Time	T_{dry bulb}	T_{sky}	W_{wind}	T_{ext rad}	H_{c,ext}
Hours	°C	°C	m/s	°C	(W/m²K)
9	-7.5	-26.1	3.8	-16.8	18.8
10	-5.0	-23.6	4.2	-14.3	20.4
11	-2.6	-22.5	4.2	-12.5	20.4
12	-1.4	-20.0	3.7	-10.7	18.4
13	-1.1	-17.1	3.7	-9.0	18.4
14	-1.6	-16.2	3.8	-8.9	18.8
15	-2.9	-16.1	3.2	-9.5	16.6
16	-4.2	-17.2	3.0	-10.7	15.9

Location: N 50° 06' E 14° 17'

Date: 21-06-2015

Table 6.4 Climate data for summer

Time	T_{dry bulb}	T_{sky}	W_{wind}	T_{ext rad}	H_{c,ext}
Hours	°C	°C	m/s	°C	(W/m²k)
9	18.8	10.6	5.4	14.7	24.6
10	19.6	11.3	5.9	15.5	26.5
11	21.1	12	5.7	16.5	25.8
12	23.1	13	5	18.1	23.1
13	24.2	15	4.2	19.6	20.4
14	24.7	16.2	3.7	20.4	18.6
15	25.1	16	3.3	20.5	17
16	25.6	15	3	20.3	16.1

The weather data were obtained from TRNSYS simulation software.

7. RESULTS

After a considerable amount of iterations in Fluent, the following results were obtained.

7.1 Air side model (4.32 mm) for summer conditions

Table 7.1 Results for wide gap (4.32mm) for summer conditions.

Time	T _{dry bulb}	T _{outlet}	ΔT
Hours	$^{\circ}\text{C}$	$^{\circ}\text{C}$	$^{\circ}\text{C}$
9	18.8	24.3	5.5
10	19.6	28.3	8.6
11	21.0	32.6	11.6
12	23.0	36.9	13.8
13	24.2	37.8	13.6
14	24.7	34.4	9.7
15	25.1	31.7	6.6
16	25.5	28.8	3.3

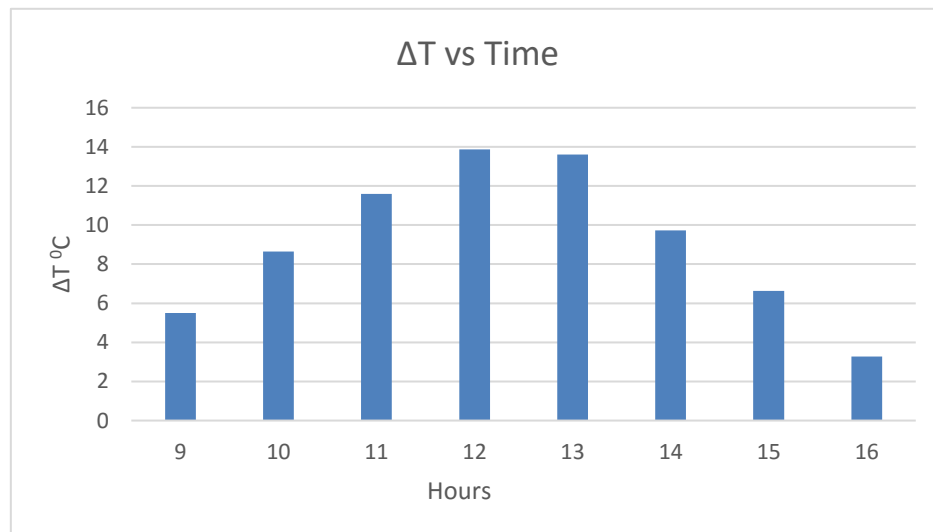


Figure 34 : Rise in air temperatures vs time (21st June)

As it could be seen that the temperature rise is maximum of around 14 $^{\circ}\text{C}$ was achieved at 12 noon.

7.2 Air side model (4.32 mm) for winter

Table 7.2 Air model for wide gap collector for winter

		Non-Selective	Selective
Time	T_{dry bulb}	ΔT	ΔT
Hours	°C	°C	°C
9	-7.5	6.6	6.3
10	-5	14.1	13.6
11	-2.6	18.4	17.8
12	-1.4	22.3	20.9
13	-1.1	18.9	18.4
14	-1.6	14.8	14.2
15	-2.8	7.1	7.1

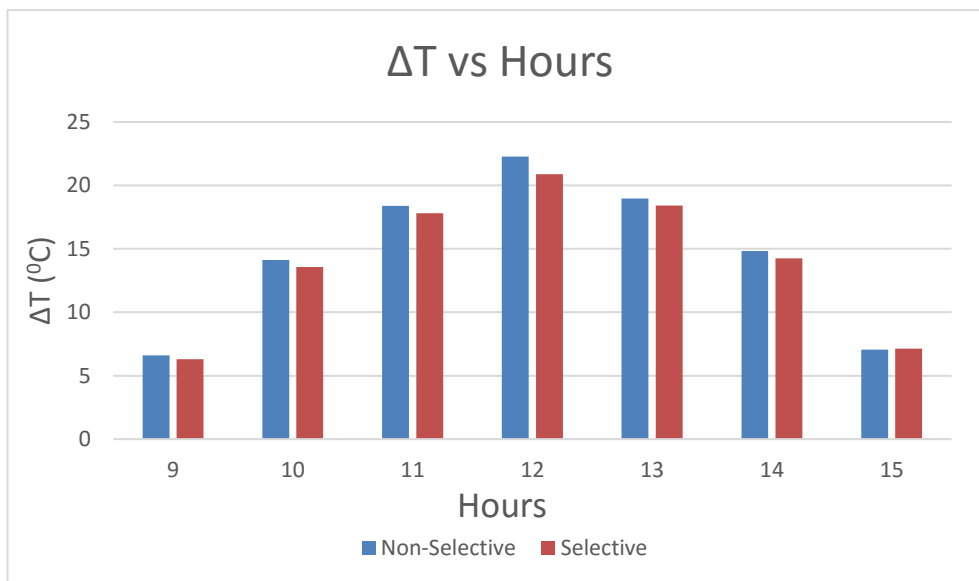


Figure 35 : Temperature rise vs hours (21st December) for wide gap

It was seen that the temperature rise is maximum around 20 °C at 12 noon. It was also observed that the collector without the selective coating gave higher temperature rise thus provided better results.

7.3 Air side model (1.41 mm) for winter

Table 7.3 Air side model for Narrow gap collector for winter conditions

	Non-selective	Selective
Time	T_{dry bulb}	ΔT
Hours	°C	°C
9	-7.5	6.1
10	-5	8.5
11	-2.6	10.7
12	-1.4	19.1
13	-1.1	18.5
14	-1.6	14.9
15	-2.9	6.9

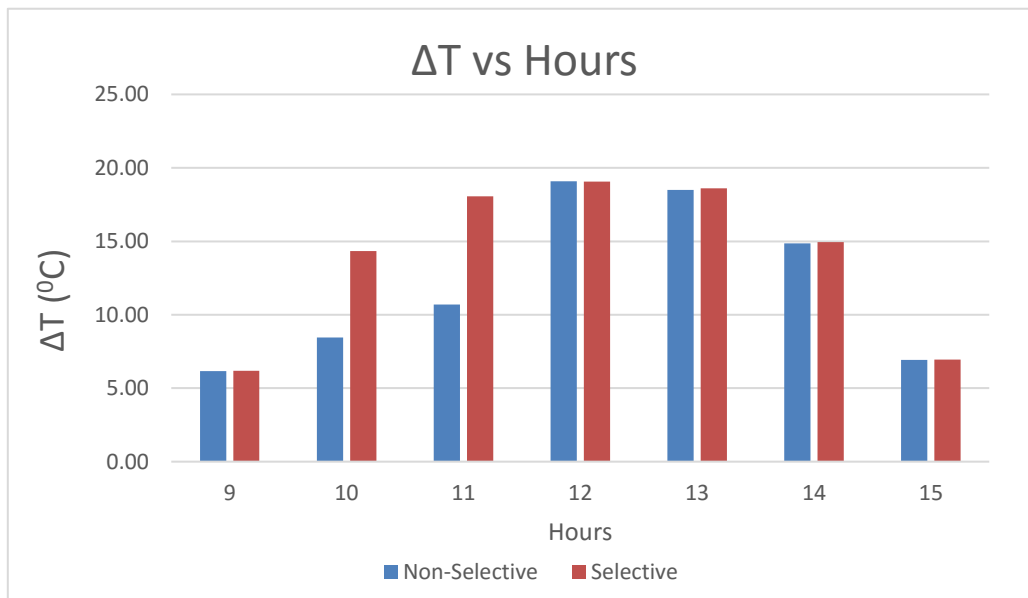


Figure 36 : Temperature rise vs hours (21st December) for narrow gap

In the narrow gap collectors, the selective and non-selective models gave similar results expect at 10:00 and 11:00 hours.

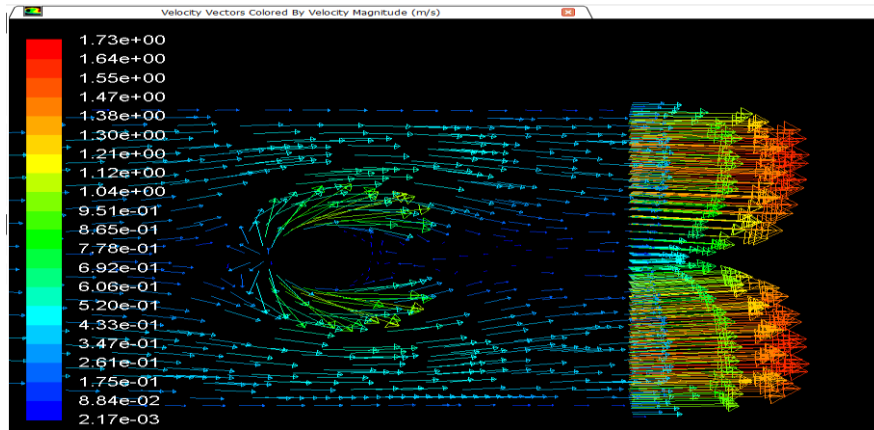


Figure 38 : Velocity (m/s) profile near the outlet of the collector.

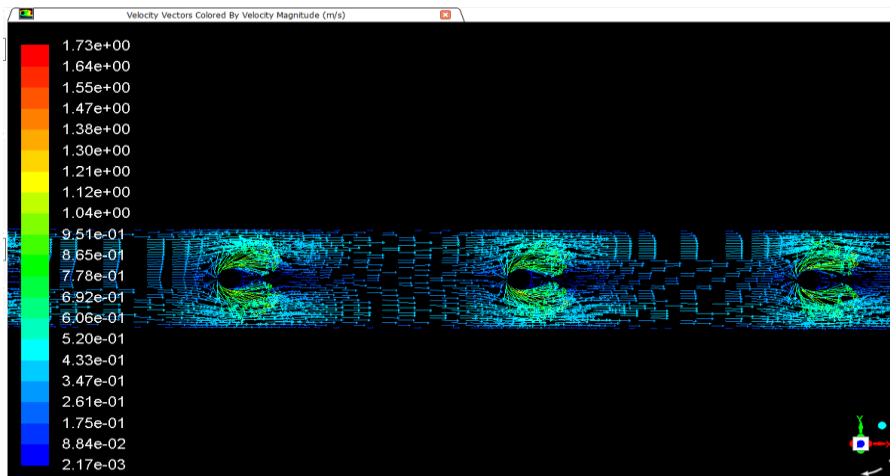


Figure 37 : Overall velocity (m/s) profile for air.

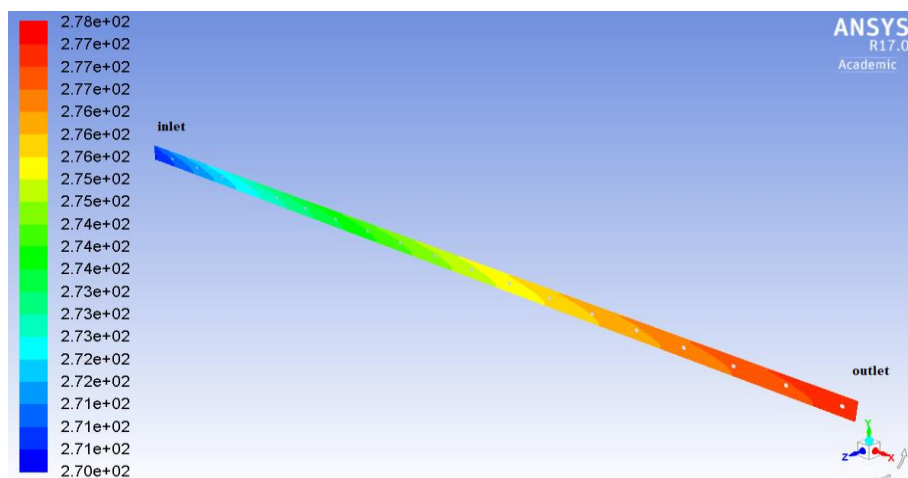


Figure 39 : Temperature (K) profile over the fins

7.4 Water side model

For water side collector, good results could not be reached. The solution for the model was not converging and the temperature of the water at the outlet of the pipes was same as the inlet temperature.

It was suggested that the geometry made for this model in the design modeler was not suitable, as the fins were made without the thickness and this thickness was represented by so-called shell conduction in Fluent. The heat could not transfer by conduction from fins to the water in pipes because of the small contact area between the fins and the pipe which is about 0.1 mm wide ring. Thus no final and definite results could be obtained from this part of the model.

7.5 Radiation gains and losses for winter conditions

As per calculation in chapter 5, the net radiation losses from the collector were found out and from the CFD fluent simulation we were able to calculate the net radiation gains.

Table 7.4 Radiation gains and losses with selective coating

Time	Gain -Wide Gap	Gain-Narrow gap	Loss-Wide gap	Loss-Narrow Gap
hours	(Watts)	(Watts)	(Watts)	(Watts)
9	444	445	27	78
10	937	994	39	114
11	1162	1243	48	138
12	1608	1551	52	140
13	1201	1224	45	130
14	944	995	37	113
15	402	463	24	69



Figure 40 : Gains and losses for collectors with selective coating on 21stDecember

Table 7.5 Radiation gains and losses with non-selective coating

Time	Gain Wide Gap	Gain Narrow gap	Loss Wide gap	Loss-Narrow Gap
hours	(Watts)	(Watts)	(Watts)	(Watts)
9	444	445	31	89
10	937	994	44	130
11	1162	1243	55	157
12	1608	1551	60	159
13	1201	1224	52	148
14	944	995	42	124
15	402	463	28	79

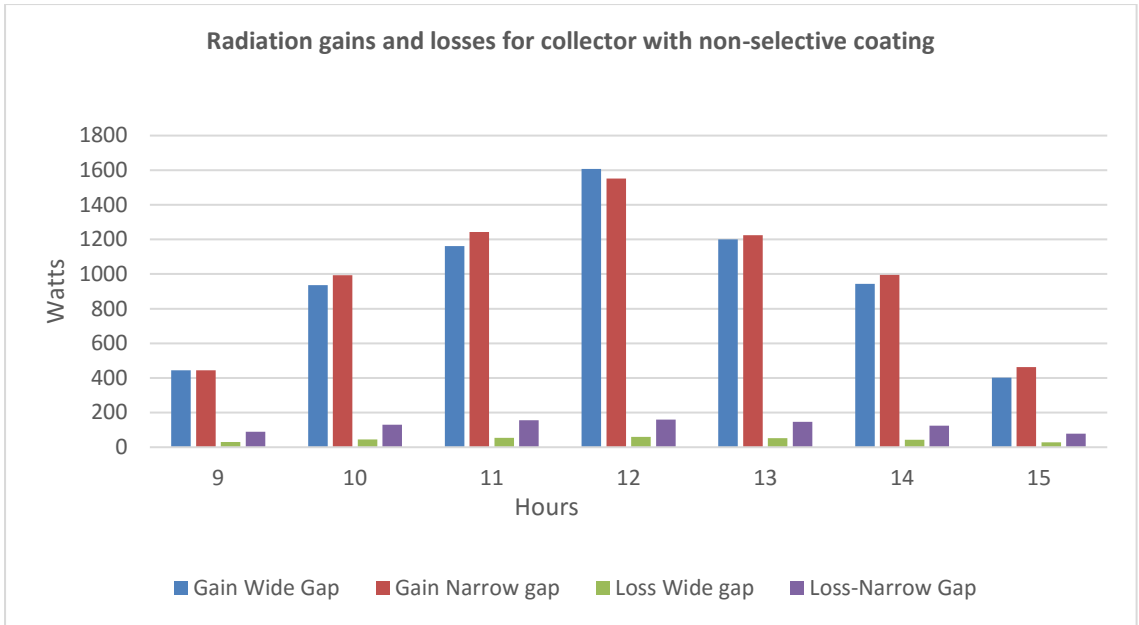


Figure 41 : Gains and losses for collectors with non-selective coating 21stDecember

7.6 Pressure loss across the air side.

From chapter 5 results, we could trace the graph of pressure drop versus the gap between the fins by keeping all other parameters constant.

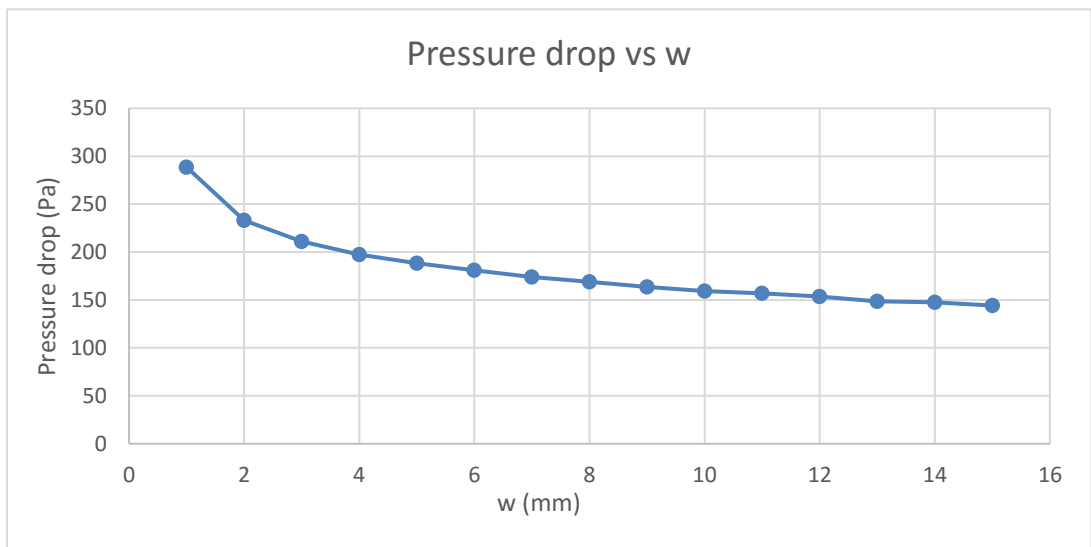


Figure 42 : Pressure drop along fins vs space between fins

From the above graph it can be seen that the pressure loss across the fins becomes almost constant after a certain gap between the fins.

7.7 Radiation losses through the fins.

Using the calculations in chapter 5, we were able to find out the radiation heat loss from a single air channel and this result was used to calculate the radiation loss through the entire collector.

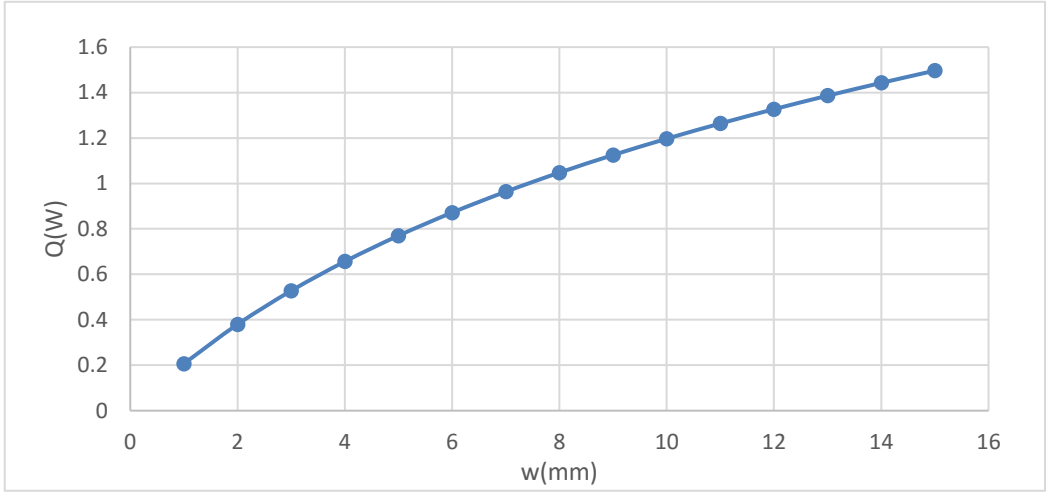


Figure 43 : Radiation heat loss from single air channel.

On varying the width between the fins also changes the number of channels in the solar collector. The graph below depicts the total heat radiated from all the fins in the collector. It can be seen as the width between the fins is increased the radiation losses are increasing.

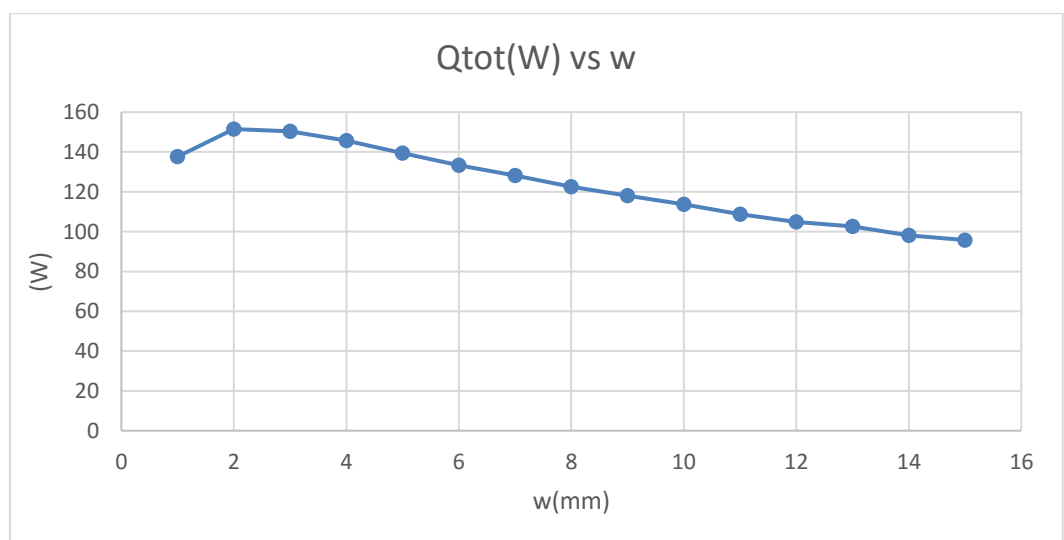


Figure 44 : Radiation loss vs fin spacing.

8. CONCLUSION

The aim of the thesis was to support the design of a dual-function solar collector by the analysis of fluid flow and heat transfer based on manual calculations and CFD simulations. It was decided to study two geometries of the collector, for the air side and for the water side of the model. Each model had fins with two spacing options. Every model was planned to be simulated with selective and non-selective coating.

ANSYS Fluent with the S2S radiation model and the Solar load model was used for the simulation of all the variants. The model for the air side geometry was simulated for summer and winter condition and showed reasonable results and the idea to replace the expensive selective coating using the fins was also verified by comparing the results from simulation of the models.

The results from the water side of the model could not to be achieved. The solution for the model was not converging and the temperature of the water at the outlet of the pipes was same as the inlet temperature. This suggests that the geometry made for this model in the design modeler was not suitable as the fins were made without the thickness and this thickness was represented by so-called shell conduction in Fluent. The heat could not be transferred from fins to the water in pipes because of the small contact area between the fins and the pipe which is about 0.1 mm wide ring. Whereas in the actual manufacturing process of fin tube heat exchanger, the pipe is pressed through a neck moulded from the fin material increasing the contact area, thus increasing the amount of heat conducted to the water through the pipe. It was also observed that the combination of laminar flow of water in the pipes and turbulent flow of air between the fins driven by buoyant forces was somewhat difficult for the Fluent solver, generating strange flow patterns inside of the pipes and therefore not reaching convergence at all.

On comparing the results of wide gap collector with selective and non-selective coating, it was analysed that the outlet air temperature hardly varied, in fact the results of collector with non-selective coating were better than the collector with selective coating except for one hour. Thus the idea of not using the selective coating and reducing the heat loss by long wave radiation by using the fins with small spacing looks to be promising.

On comparing the results of wide gap and narrow gap, again the wide gap collector had slightly higher outlet air temperature. This would be because of lower radiation losses from wide gap collector. Thus the result obtained from the manual calculation coincided with the simulation results. As the gap between the fins decreases, the number of channels in the collector is increased, so despite of radiation losses being less from a single narrow gap, the total radiation losses from the collector is higher. The wide gap collector has lesser number of fins and lesser weight. Thus saving up on the cost of material and also saving up on not using the selective coating.

It can be suggested that the wide gap collector had pretty good results even without the use of the selective coating. The use of this expensive selective coating can be avoided and also the wide gap fins compared to the narrow gap can save up on a lot of material used and reduce a considerable amount of weight of the collector. Also the construction of this collector is similar to the fin tube heat exchangers available in the market, thus the manufacturing of this collector could be done using the currently available processes.

These hybrid collectors can be used throughout the year compared to the currently available and installed single purpose collectors. They can be used for domestic hot water preparation in the summer, can be used in combination with heat pumps and for ventilation in the winter.

It can be recommended that in any future CFD investigation of the water side model, rather than using the shell conduction approach, a geometry with thicknesses for the fin and pipes should be prepared. The contact surface area between the fins and the pipes should be higher resembling the designs which are available in the market.

9. BIBLIOGRAPHY

- Assari, M., Basirat, H., Tabrizi, b., Jafari, I. (2011), Experimental and theoretical investigation of dual purpose solar collector, *Solar Energy* 85 Pg.601–608
- Chow, T. (2009), A review on photovoltaic/thermal hybrid solar technology, *Applied Energy* Vol.87, Pg.365–379.
- Jafari, I., Ershadi, A., Najafpour, E., and Hedayat, N. (2011) Energy and Exergy Analysis of Dual Purpose Solar Collector, *International Journal of Mechanical, Aerospace, Industrial, Mechatronic and Manufacturing Engineering* Vol:5, No:9, Pg. 1712-1714
- Jie J., Chenglong, L., Chow, T, Wei, S., Wei, H. (2011) Thermal characteristics of a building-integrated dual-function solar collector in water heating mode with natural circulation. *Energy* 36(1), Pg.566-574
- Jie, J., Chao, G., Wei, S., Wei, H., Yanqiu, W., Guiqiang, L. (2014) Experimental investigation of tri-functional photovoltaic/thermal solar Collector, *Energy Conversion and Management* 88 Pg. 650–656
- Jinwei, M, Wei, S., Jie, J. (2011) Experimental and theoretical study of the efficiency of a dual-function solar collector, *Applied Thermal Engineering* 31 Pg. 1751-1756
- Matuska, T. (2016), Design concept for dual-function solar collector.
- Qahtan, A, Viorel, B., Iuliana, S. (2015) Hybrid solar collector for water and air heating: effects of storage tank volume and air channel shape on efficiency, *U.P.B. Sci. Bull., Series D, Vol. 77, Iss. 3, Pg. 29-40*
- Saleh, A., Jasim, M. (2014) Experimental Study of The Performance of The Dual Purpose Solar Collector, *Eng. & Tech. Journal* , Vol.32, Part (A), No.11,P. 2673-2683
- Venu, A., Arun, P. (2013) Simulation Studies on Porous Medium Integrated Dual Purpose Solar Collector, *International journal of renewable energy research* vol.3, no.1, Pg.114-120
- Wei, H., Hong, X., Luo, B., Hongbing, C., Jie, J. (2016) CFD and comparative study on the dual-function solar collectors with and without tile-shaped covers in water heating mode. *Renewable Energy* Vol.86, Pg.1205-1214.